MLM-1231

MOUND LABORATORY PROGRESS REPORT FOR DECEMBER, 1964

J. F. Eichelberger, G. R. Grove and L. V. Jones

AEC Research and Development REPORT

MONSANTO RESEARCH CORPORATION

A SUBSIDIARY OF MONSANTO COMPANY

MOUND LABORATORY

MIAMISBURG, OHIO

OPERATED FOR

UNITED STATES ATOMIC ENERGY COMMISSION

U.S. GOVERNMENT CONTRACT NO. AT-33-1-GEN-53

DISCLAIMER

MLM-1231
TID-4500 (37th Ed.)
Category - UC 2
Progress Reports

MOUND LABORATORY PROGRESS REPORT FOR DECEMBER, 1964

J. F. Eichelberger
G. R. Grove
L. V. Jones

Date: December 21, 1964
Issued: April 7, 1965

The Mound Laboratory Progress Report, issued monthly, is intended to be a means of reporting items of current technical interest in research and development programs. To issue this report as soon as possible after the end of the month, editorial work is limited; and since this is an informal progress report, the results and data presented are preliminary and subject to change.

These reports are not intended to constitute publication in any sense of the word. Final results either will be submitted for publication in regular professional journals or will be published in the form of MLM topical reports.

The previous reports in this series are:

MLM-1227	MLM-1192
MLM-1221	MLM-1185
MLM-1217	MLM-1183
MLM-1216	MLM-1179
MLM-1209	MLM-1178
MLM-1204	MLM-1177
MLM-1203	MLM-1176
MLM-1196	

MONSANTO RESEARCH CORPORATION

A SUBSIDIARY OF MONSANTO COMPANY

MOUND LABORATORY

MIAMISBURG, OHIO

OPERATED FOR

UNITED STATES ATOMIC ENERGY COMMISSION

U.S. GOVERNMENT CONTRACT NO. AT-33-1-GEN-53

TABLE OF CONTENTS

SUMMARY

RADIOELEMENTS

Uranium-234 The study of tri-n-octylphosphine oxide (TOPO) in a proposed uranium-234 recovery process was continued. Increased organic loading by multiple extractions was demonstrated, with acceptably low uranium losses. Recovery of uranium-234 from waste ion exchange raffinates in a two-cycle batch TOPO solvent extraction process was studied.

Hydrolytic Separations of Protactinium Milligram amounts of protactinium-231 can be separated from its decay products, actinium-227, thorium-227, and radium-223, by hydrolysis from 1*M* and 6*M* hydrochloric acid. Separation from milligram amounts of thorium is accomplished by hydrolysis in 1*M* nitric acid, and from niobium by hydrolysis in a mixture of oxalic and hydrochloric acids. Iron is separated by selective dissolution of its hydroxide in dilute hydrochloric acid. Microgram amounts of protactinium are separated from its decay products by adsorption on glass wool from a dilute sulfuric acid solution and by the method of residue adsorption and selective desorption from a gold surface. The application of the adsorption technique to the problem of "inextractable polymers" is discussed briefly.

Polonium-208/Polonium-209 Relative radial distribution curves of the isotopic mixture of polonium-208 and polonium-209 have been obtained from x-ray diffraction patterns of the metal at room temperature. Po-Po interatomic distances were observed at 3.5A, which were in good conformity with the sum of Pauling's metallic radii of 3.52A. The octahedral configuration of six polonium atoms around the central polonium was indicated by the octahedral edge distance of 4.9A.

ISOTOPE SEPARATION AND PURIFICATION

Carbon-13 The 12-column, 8-stage methane thermal diffusion system is again in equilibrium operation following the column inventory loss in August, 1964. Withdrawal of product at a mass-17 enrichment greater than 98% was resumed in December, 1964. The capacity of the conversion system was increased to 0.7 gram of carbon-13.

The separation factor of the carbon dioxide-monoethanolamine exchange system was increased from 1.10 to 1.20, a 20% improvement.

Helium Degassing of a long charcoal trap was found to be ineffective when the trap was used in reducing the tritium concentration to a level of 10^{-16}%. A cylindrical charcoal trap is being tested.

Neon A revised arrangement of four columns in cascade with partially enriched neon-21 feed has enriched the neon-21 to 19%.

Argon With argon-36 product of more than 99.98% being drawn from the top of a four-stage cascade system at 1.8 ml/hr, the concentration of argon-38 at the bottom of the third stage has increased to 9% from a natural abundance of argon-38 of 0.06%.

Krypton The two-stage cascade enriched the heavy isotopes krypton-84 and -86. The product averaged 28% krypton-86.

A detailed program for the preparation of krypton gas depleted in krypton-85 was prepared, including a method of predicting the krypton-85 content by using mass spectrometric analysis of the other stable isotopes.

Xenon The six-stage cascaded thermal diffusion system with two swing units was restarted using fresh fission feed.

Experiments using argon as the carrier gas in krypton-xenon separation by gas chromatography were performed. The use of this gas is not recommended.

Thermal Diffusion Research The basic construction of the single-beam production apparatus was completed and preliminary runs were made to ascertain adjustment procedures. Adjustments are now being made to produce a balanced detection system between the two opposed ionization gauge tubes. The differential reading between these tubes is monitored on a dual-input recorder along with the corresponding source pressure readout.

Transport coefficient measurements for neon and methane were obtained and compared with theory. The agreement is good.

Helium Research A single run was made on the vapor pressure thermometry apparatus using unsaturated helium-4 in the bulb and liquid helium-4 in the cooling baths. The discrepancy between Mound Laboratory measurements of helium-3 and helium-4 vapor pressure corrections due to thermal transpiration and the predictions of the Weber-Schmidt equation still cannot be resolved. Efforts are being made to check all phases of these precise measurements in order to fully back up the experimental values.

ANALYTICAL AND INSTRUMENTATION

Neptunium Analysis Neptunium(V) can be separated from plutonium(IV), thorium(IV) and uranium(VI) by a method of solvent extraction. The acidity of the nitric acid media should be less than 0.2*M* in order to obtain a separation of 99%. The neptunium is extracted with tri-n-octylphosphine oxide from 1*M* HNO_3 containing ferrous sulfamate. The neptunium is measured by a spectrophotometric procedure using arsenazo to develop a colored complex.

Cobalt Analysis A method for the spectrophotometric measurement of cobalt in plutonium metal was developed. A color reagent, nitroso-naphthol, which is specific for cobalt was used. Plutonium does not interfere with the determination.

Analysis of Enriched Uranium-234 for Comparison Purposes An isotopic analysis of the uranium-234 content of a sample of enriched uranium was made according to a specified analytical method. The uranium-234 content was found to be 1.51 wt %. Alpha pulse height analysis of the sample gave a value of 0.98 wt % uranium-234. Alpha pulse height analysis of NBS standard uranium (U_3O_8) gave 0.0053 wt % uranium-234, as compared to a literature value of 0.0057 wt %.

Analysis of Stearic Acid in Silver Powder The stearic acid content of silver powder was determined by a method of pyrolysis combined with gas chromatography using a silica gel column.

Nuclear Magnetic Resonance Studies Complex formation between tri-n-octylphosphine oxide (TOPO) and 77 metals in the form of their inorganic salts was studied by NMR. Complex formation was indicated by a chemical shift change between the absorption peaks of the methyl-group (CH_3-) protons and the terminal methylene (-CH_2-) protons adjacent to the phosphorus oxide group of the TOPO molecule. The magnitude of the chemical shift change appears to be directly proportional to the amount of metal complexed to TOPO. The NMR data also indicate that the metal and the TOPO molecule are undergoing rapid exchange, with the result that all the TOPO molecules appear to be complexed with a metal atom.

Semiconductor Radiation Detectors Techniques of fabrication of germanium semiconductor radiation detectors are being developed for use at cryogenic temperatures. Detectors on hand which have been overexposed to radiation can frequently be reworked by relatively simple techniques. Also these techniques can be used to prepare other types of detectors which are not commercially available.

A silicon surface barrier detector was fabricated by these experimental techniques, and an alpha particle energy resolution of better than 4% FWHM (full width, half maximum) was obtained for a polonium-208 -209 -210 sample.

Calorimetry The construction of a closed-loop servo control system is illustrated by the detailed description of an environmental water bath temperature controller. The system consists of a temperature sensor, a battery device Wheatstone bridge, and an amplifying system and heater.

A water-bath calorimeter capable of assaying 450 watts of power has been constructed and used to assay 300-watt samples of polonium-210. The calorimeter is constructed to operate according to a method that was developed at Mound Laboratory in 1956 to measure heat capacities.

RADIOELEMENTS

Basic and applied research is being conducted on a number of radioelements to determine their physical properties, to develop analytical techniques, and to study the basic radiochemistry involved. Of particular interest are alpha emitters, their decay chains, their isotopes, and their chemical homologs.

URANIUM-234

A study of tri-n-octylphosphine oxide (TOPO) in a proposed uranium-234 recovery scheme was continued.

Previous work had indicated that the capacity of the organic extractant was much greater than the expected quantities of uranium in the feed solution. Series of extractions were performed to determine the feasibility of increased organic loadings. A feed solution (1.5 liters) containing 10 micrograms of uranium per milliliter in 7.2*M* nitric acid was prepared. One hundred fifty milliliters of solution were extracted with 50 milliliters of 0.1*M* TOPO in Amsco (aqueous organic ratio 3) by stirring for 15 minutes and settling for 15 minutes before removing the aqueous phase. Successive 150-milliliter portions of feed solution were extracted with the same organic solution until the entire feed solution was processed. Samples of each aqueous raffinate were taken and the residual uranium was determined by the PAN Method.[1] The results of duplicate series are shown in the second and third columns of Table 1. The effect of impurities was determined by preparation of another feed solution containing uranium (10 micrograms/milliliter), ferric nitrate, cupric acetate, cobaltous chloride, nickel sulfate, aluminum nitrate, (each 0.01*M*) and sodium fluoride (0.001*M*) in 7.2*M* nitric acid. This solution was extracted exactly as before, and the results of the uranium determinations are listed in the fourth column of Table 1. In each of the three series, the percentage loss of uranium in a single stage was quite low for the early extractions and increased gradually to nearly 20% in the tenth extraction. In each case losses from the extraction of the feed containing impurities (series C) were slightly higher, but the maximum loss was still less than 20%. Variations of the results for series A and B are attributed to small differences in the extraction and analytical procedures and are indicative of the precision of the determinations. The accumulative losses in each series were calculated and are listed in the last three columns of Table 1. These data predict that 8 to 10 extractions with an overall yield of 90% are possible, depending upon the impurities in the feed solution.

After each series of extractions, the loaded organic was stripped with 17 milliliters of 1*M* sodium carbonate (organic/aqueous ratio = 3). Approximately 1% of the uranium remained in the organic phase. No precipitates were formed in the stripping step although the spectrum of the organic used in series C (with impurities) showed an additional peak caused by extracted iron. Thus multiple extractions to increase the loading of the organic phase should be feasible in the recovery process.

A number of other extractants were scanned to determine their suitability in a uranium-234 recovery system. Trioctylmonomethyl ammonium chloride proved to be intractable due to its high viscosity, and tetraheptyl ammonium iodide was insoluble in all of the common solvents tried; therefore these two extractants were not considered further. Solutions of several organophosphorus compounds were prepared in Amsco and were contacted with a solution of uranium in 6.6*N* HNO_3. Uranium remaining in the aqueous phase was determined and the results are listed in Table 2 along with the calculated distribution coefficients. As a comparison, a 0.1*M* TOPO extraction was also performed. The results indicate that TOPO is still the best extractant, although di-(2-ethylhexyl) phosphoric acid and dibutyl butylphosphonate could be considered as alternates.

[1] R. J. Baltisberger, *Anal. Chem.*, 36, 2369 (1964).

Table I

URANIUM LOSSES

Extraction	Uranium Left in Raffinate			Accumulative Losses		
	Series A (%)	Series B (%)	Series C (%)	Series A (%)	Series B (%)	Series C (%)
1	0.8	1.3	3.9	0.8	1.3	3.9
2	2.8	2.9	5.7	1.8	2.1	4.8
3	5.2	3.9	6.3	2.5	2.7	5.3
4	8.2	6.8	7.7	4.3	3.7	5.9
5	8.0	8.6	9.9	5.0	4.7	6.7
6	11.6	10.6	12.7	6.1	5.7	7.7
7	12.4	12.6	14.8	7.0	6.7	8.7
8	14.8	14.8	14.3	8.0	7.7	9.4
9	16.4	17.0	19.3	8.9	8.7	10.5
10	17.2	18.7	19.5	9.7	9.7	11.4

Table 2

COMPARISON OF URANIUM EXTRACTANTS[a]

Extractant	Organic Conc.	Uranium In Raffinate (%)	D o/a[b]
Di-(2-ethylhexyl) phosphoric acid	10 vol%	0.90	111
Dibutyl butylphosphonate	10 vol%	1.63	61
Dibutyl benzenephosphonate	10 vol%	6.7	14
Di-2-ethylhexylphosphite	10 vol%	15.2	6
Tri-n-octylphosphine oxide (TOPO)	3.9 wt%	0.71	145

[a]Organic/aqueous ratio 1.
Aqueous phase: 10 ml 6.6\ HNO_3; 10.15 mg uranium.
Shaking phases 2 minutes; settling 15 minutes.

[b]Distribution coefficient.

HYDROLYTIC SEPARATIONS OF PROTACTINIUM

The well-publicized tendency of protactinium to hydrolyze has usually been regarded as a burden to be circumvented or tolerated. Relatively little attention has been given to the useful aspects of this behavior. Some of the separations made possible by the hydrolytic and adsorptive tendencies of protactinium are described and some of their fundamental implications are pointed out.

General Procedure for Hydrolytic Separations The source material was a four-year old solution containing approximately 90 milligrams of protactinium per milliliter in approximately 5*N* H_2SO_4. Each sample consisted of 25 microliters of this solution containing 2.4 mg of Pa^{231}, 1.5 ng of Ac^{227}, 0.35 pg of Th^{227}, and 0.21 pg of Ra^{223} in equilibrium with the short-lived decay products.

Each separation was performed in a 15-ml graduated Pyrex centrifuge tube. Addition of reagents was made at room temperature (~25 C) with vigorous mechanical stirring, after which the tube was heated at 98°C in a thermostatically controlled heating block for at least 15 minutes. Heating, with occasional manual swirling to disperse the flocculent precipitates, was continued until the precipitate settled, leaving a clear supernate.

The centrifuge tube was removed from the heat, and the solution was stirred mechanically for 15 minutes at room temperature. After centrifugation, the supernatant liquor was removed with a transfer pipette and passed through Whatman #42 filter paper into a 10-ml volumetric flask. If a second precipitation was carried out, the same procedure and filter were used, and the supernate and or washings were combined in the same volumetric flask.

Protactinium was recovered from the centrifuge tube by dissolution at room temperature with 1 ml of 0.1*N* HF. The solution was passed through the same filter as that used for the supernate, and the filtrate was collected in a second volumetric flask. The tube, glassware, and filter were washed with 0.01*N* HF to yield a total of 10 ml of 0.02*N* HF. The centrifuge tube, stirring rod, transfer pipette and filter were checked for residual radioactivity by gamma-counting in a 3- x 3-inch NaI(Tl) well crystal.

Separation from Niobium The protactinium sample was mixed with 2 mg of niobium (as niobium oxalate) and a tracer amount of Zr^{95}/Nb^{95} in 1.5 ml of 0.1*N* $H_2C_2O_4$. The slightly turbid solution was cleared by heating for a few minutes in the heating block. One ml of 1*N* $H_2C_2O_4$ was added, and the volume was adjusted to 3 ml with demineralized water.

The solution was stirred vigorously, and 1 ml of 6*N* HCl was added slowly. The clear solution was heated and became turbid within 5 minutes. A precipitate settled out within 10 minutes. Heating was continued for a total of 20 minutes. The solution was cooled, centrifuged, and decanted.

The precipitate was washed by stirring it with 0.1*N* HCl for a few minutes at room temperature, then centrifuged. The supernate was decanted through the same filter, and the filter was washed with 0.1*N* HCl to the 10-ml volume. Protactinium was recovered in 10 ml of 0.02*N* HF.

Gamma spectra of the two solutions (Figure 1) showed that 2.0% of the niobium remained in the protactinium fraction. The niobium fraction contained (by alpha spectrometry) 5.6% of the protactinium, all of the radium-223, and approximately 40% of the thorium-227.

Separation from Thorium The protactinium sample was mixed with 2.5 mg of thorium (as thorium nitrate) in 0.25 ml of 1*N* HNO_3. The slightly turbid mixture was diluted to 4 ml with 1*N* HNO_3, stirred briefly, and covered to reduce evaporation. The solution was heated, and a precipitate settled out within 5 minutes. Heating was continued for a total of 30 minutes. The solution was cooled to room temperature, centrifuged and decanted.

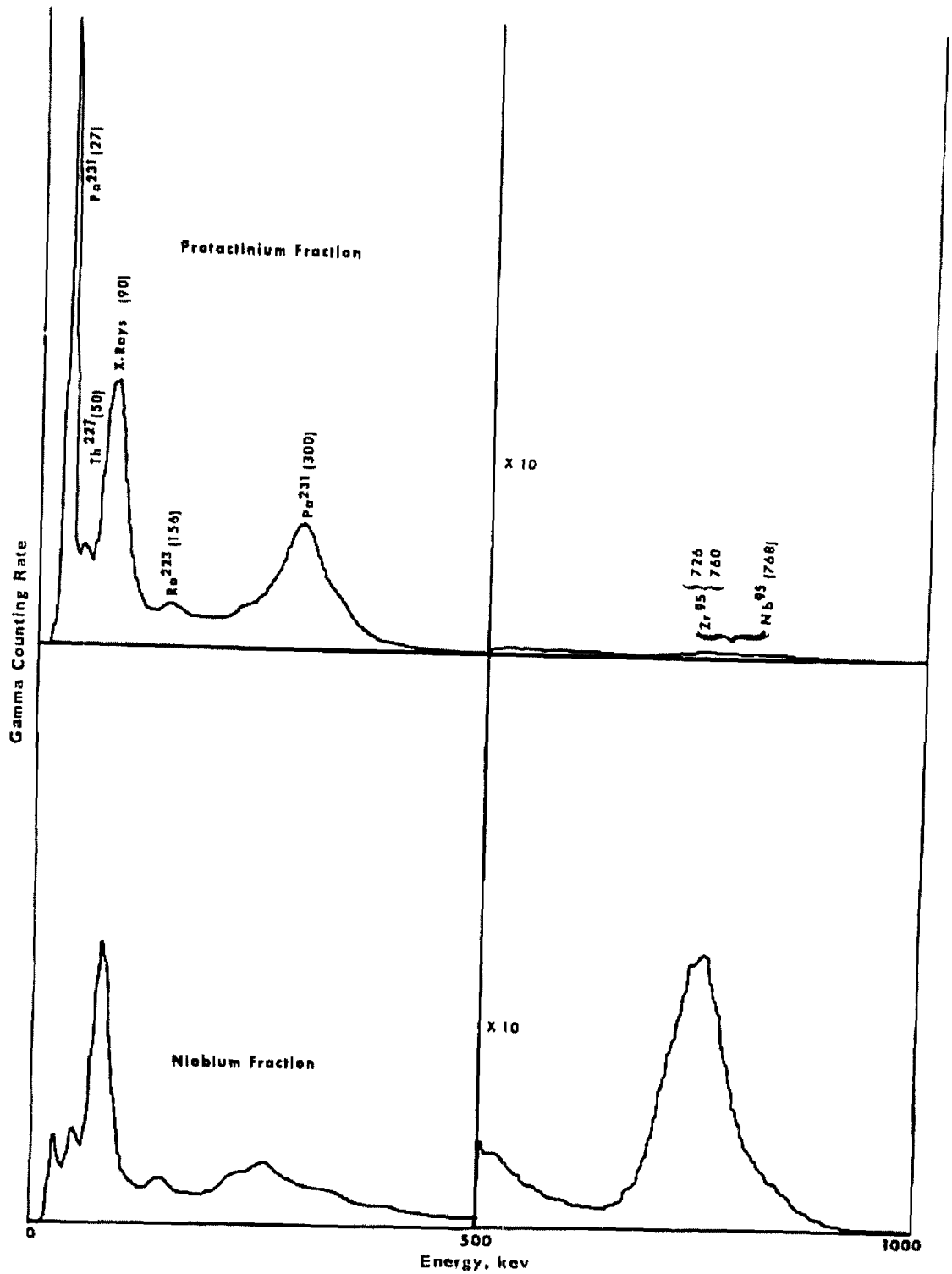

Figure 1. *Gamma Spectra of the Niobium and Protactinium Fractions*

The precipitate was washed by stirring with 4 ml of 1% HNO_3 for 5 minutes at room temperature. The slurry was centrifuged, and the supernate was decanted through the same filter. The filter was washed with 1% HNO_3, and the combined supernate and washings were brought to a volume of 10 ml. The protactinium was recovered in 10 ml of 0.02% HF.

On the basis of the thorium-227 content, the protactinium fraction contained 1.7% of the thorium, and the thorium fraction contained 0.4% of the protactinium.

Separation from Decay Products The protactinium sample was diluted with 1% HCl to a total volume of 4 ml. A precipitate developed immediately. The solution was stirred, heated for 15 minutes, cooled, centrifuged and decanted.

The precipitate was redissolved by heating for a few minutes with 0.1 ml of 6% H_2SO_4. The solution was cooled, and the precipitation from 1*N* HCl was repeated.

Gamma spectrometry showed the presence of residual thorium-227 on the filter, but no protactinium. Of the total thorium-227 in the filtrates, 7.9% was found (by alpha spectrometry) in the protactinium fraction; 0.7% of the protactinium was found in the decay product fraction.

In a second experiment, the 1% HCl precipitate was redissolved by stirring vigorously with 2 ml of 12*N* HCl at room temperature. After 45 minutes, only a slight turbidity remained. Demineralized water was added dropwise with continuous stirring, and a precipitate developed immediately. The volume was increased to 4 ml with water (yielding 6% HCl), and the solution was heated, cooled, centrifuged, and decanted as before.

Residual thorium-227 was again detected on the filter paper, but not protactinium. The protactinium fraction contained 1.1% of the thorium-227, but none of the radium-223. Actinium-227 could not be accurately determined because of interference by the 4.94-Mev alpha peak of protactinium, but it was estimated that essentially all of it was in the supernatant solutions. The combined supernates contained 2.1% of the protactinium.

Separation from Iron by Selective Dissolution A solution was prepared containing 1 mg of Pa^{231} and 1 mg of Fe (plus Fe^{59} tracer) in 5.5 ml of 0.3*N* HCl/0.02*N* HF. The iron and protactinium were coprecipitated as hydroxides by the addition of 2 ml of 3*N* NH_4OH. The solution was stirred for 5 minutes at room temperature and centrifuged. The supernate was decanted without filtration.

Two drops (0.1 ml) of 12*N* HCl were added to the precipitate; the centrifuge tube was shaken until the iron dissolved. The solution was diluted to 4 ml with 0.1*N* HCl, stirred briefly and centrifuged. The supernate was decanted through Whatman #42 filter paper to a 10-ml volumetric flask. The remaining precipitate was stirred briefly with 2 ml of 0.1*N* HCl and centrifuged. The supernate was decanted through the same filter, and the filter was washed with 0.1*N* HCl to bring the total volume to 10 ml.

The protactinium was redissolved, as usual, in 1 ml of 0.1*N* HF and transferred, without filtration, to a volumetric flask. The centrifuge tube, stirring rod, and transfer pipette were washed with 0.01*N* HF, and the washings were combined with the solution of the principal protactinium fraction.

The filter paper was washed with 0.02% HF, and the washings were collected separately. The distribution of protactinium and iron in the various fractions is given in Table 3.

Table 3

DISTRIBUTION OF PROTACTINIUM AND IRON

Fraction	Protactinium (% of total)	Iron (% of total)
NH_4OH decantate (unfiltered)	- -	0.6
HCl solution (filtered)	4.0	95.8
HF solution of precipitate (unfiltered)	92.2	0.4
HF wash of filter	3.7	3.1

Separation from Decay Products by Adsorption on Glass Wool The protactinium source used in the hydrolysis experiments was diluted with 6% H_2SO_4 to yield a sample containing 20 μg of protactinium in 0.05 ml. The sample was diluted with demineralized water to a volume of 5 ml, mixed, and heated for 20 minutes. The solution was removed from the heat, covered, and allowed to stand at room temperature for 5 days. Upon centrifugation, there was no visible precipitate.

The solution was passed through a coarse filter, prepared by inserting a plug of Pyrex glass wool in the end of a medicine dropper and tamping it until 1.5 ml of water would drain by gravity flow in approximately 1 minute. The centrifuge tube and filter were washed with 2 ml of demineralized water and 3 ml of 0.1*N* HCl. The combined filtrate and washings were diluted to 10 ml in a volumetric flask.

Gamma spectroscopy showed that almost none of the protactinium remained in the centrifuge tube. The tube and filter were washed with 0.01*N* HF, and the solution was diluted to 5 ml in a volumetric flask.

The HF solution contained (by alpha spectrometry) 10.7% of the thorium-227, 5.4% of the radium-223, and 99.9% of the protactinium-231.

Separation from Decay Products by Residue Adsor on A synthetic mixture of protactinium-231 and its decay products was prepared as follows: A solution containing 0.75 ng of Ac^{227} in equilibrium with Th^{227} and Ra^{223} was deposited in the center of a gold-plated copper disk in 0.2 ml of 0.5*N* HNO_3. The solution was evaporated to dryness at 98°C, and the residue was covered with 0.1 ml of 0.01*N* HF containing 6 μg of Pa^{231}. This solution was dried, and the residue was redissolved in a mixture of 0.2 ml of 1*N* HNO_3 and 0.05 ml of 1*N* HF. When this solution was dry, the residue was covered with 0.2 ml of 0.1*N* HNO_3, which was heated for 1 minute at 98°C. One drop (0.05 ml) of 3% NH_4OH was added, and the solution was evaporated to dryness. The NH_4NO_3 residue was covered with 0.25 ml of 3*N* NH_4OH and dried at 98°C.

The disk was removed from the heat and allowed to cool to room temperature. The NH_4NO_3 was desorbed in 0.25 ml of 3% NH_4OH, which was transferred to a second disk. The residue was washed twice more with 0.25-ml portions of 3*N* NH_4OH, each wash being allowed to stand at room temperature until the previous desorbate had dried. The original disk was heated briefly to drive off residual moisture.

The transfer pipette was rinsed with demineralized water and this solution was deposited on a third disk. The residue on the original disk was washed three times with 0.25-ml portions of 0.1 N HNO_3, and the washings were deposited on the third disk, each wash being allowed to stand on the residue until the previous desorbate was dry. The original disk was dried at 98 C. The residue was covered with 0.25 ml of 1 N HF and heated until it was dry. The disk was removed from the heat and allowed to cool to room temperature. The residue was washed three times with 0.25-ml portions of 0.01 N HF, which were transferred successively to a fourth disk. The distribution of the various nuclides, based on alpha spectra of the four disks (Figure 2), is given in Table 4.

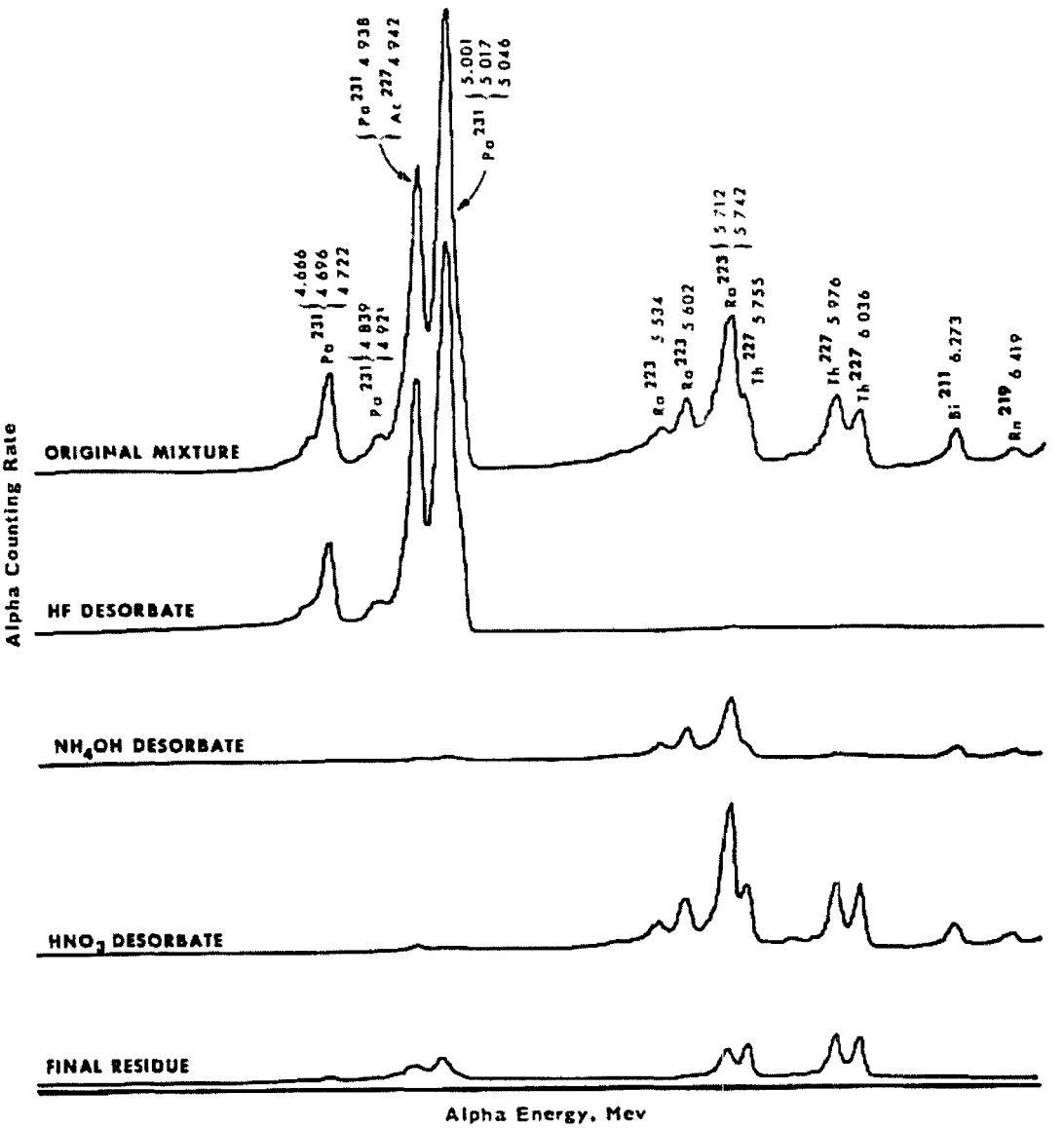

Figure 2. *Comparison of Alpha Spectra of the Four Disks*

Table 4

DISTRIBUTION OF VARIOUS NUCLIDES

Fraction	Percent of Total			
	Pa	Ac^{a}	Th	Ra
NH_4OH desorbate	1.4	6.2	4.6	35.0
HNO_3 desorbate	0.8	44.1	57.7	58.6
HF desorbate	92.2	(0.0)[a]	1.1	2.0
Final residue	5.6	49.7	36.6	4.4

[a]Because of interference between the 4.94-Mev alpha energies of Pa^{231} and Ac^{227}, the distribution is based on the assumption that no Ac^{227} was desorbed by HF; all other values are computed from the ratio between the areas under the peaks at 5.01 and 4.94 Mev.

Discussion These experiments illustrate somewhat different applications of the hydrolytic and adsorptive tendencies of protactinium to its separation from other elements.

Iron is of interest, both because of its ubiquity in nature and because ferric hydroxide is an excellent scavenger for many trace elements in solution, including protactinium. Its separation from protactinium is based on its relatively strong complex formation with chloride ion, while in contrast protactinium is essentially inert in dilute hydrochloric acid.

The solubility of protactinium in oxalic acid and its hydrolysis upon the addition of hydrochloric acid has been noted by Bouissières and Odiot.[2] The application of this behavior to the separation of protactinium from niobium is examined in more detail in another report.[1] Obviously, iron and a number of other elements which form stable oxalate complexes would be separated under the same conditions. On the other hand, thorium, which is precipitated by oxalate ion, is adsorbed or coprecipitated even at trace levels.

Like protactinium, thorium has a strong tendency to hydrolyze[4], but its hydrolysis is easily controlled by acidification, permitting a rather simple separation from protactinium.

There is strong evidence from older work[5] on "radiocolloids" and from recent publications on residue adsorption[6,7], that precipitation and adsorption are merely different aspects of the same basic phenomenon.

[2]G. Bouissières and S. Odiot, *Bull. soc. chim. France*, 1951, 918 (5) 18.

[3]H. W. Kirby and P. E. Figgins, *Purification of Protactinium from Natural Sources*. Paper to be presented at the Colloquium on Physical Chemistry of Protactinium, July 2-8, 1965, at Paris, France.

[4]E. K. Hyde, *The Radiochemistry of Thorium* Natl. Acad. of Sciences- Natl. Research Council NAS-NS 3004, p. 9 (January, 1960).

[5]G. K. Schweitzer and W. M. Jackson, *J. Chem. Educ.*, 29, 513 (1935).

[6]H. W. Kirby, *J. Inorg. & Nuclear Chem.*, 25, 483 (1963).

[7]H. W. Kirby, U.S.A.E.C. Report TID-7675, p. 122 (February, 1964).

It may be stated categorically that adsorption from solution never occurs except under conditions which would also produce precipitation if the concentration of the adsorbed species were sufficiently high. Conversely, it may be stated that desorption will take place only to the extent that the adsorbed species exhibits true solubility in the desorbing solvent. It is noteworthy that the adsorption of protactinium from organic solvents or from appropriate concentrations of hydrofluoric, sulfuric, or oxalic acid solutions is negligible.

The absence of a visible precipitate, or its failure to be brought down by centrifugation after a long period of "aging", is no assurance of true solution. When researchers resort to such subterfuges as working rapidly to evade the typically slow hydrolysis of protactinium or storing aqueous solutions in hydrophobic containers to avoid adsorption, serious limitations are imposed on the validity of the data and on the conclusions derived.

Although the separations described here were performed at relatively low acid concentrations, Moore and Rainey[9] have demonstrated the quantitative adsorption of trace quantities of protactinium-233 and up to 0.0002*M* protactinium-231 from nitric acid solutions as concentrated as 11*M*. They also report that an increase in thorium concentration at constant acidity substantially decreases the adsorption of protactinium. It may be predicted, therefore, that even at high acidities, a reduction in ionic strength would result in the precipitation of protactinium, a prediction borne out by the observations of Hardy and Scargill[9] on the depolymerization of protactinium by dilution with nitric acid.

The conditions which favor the adsorption of protactinium are the same as those which yield "inextractable polymers", and the mechanisms are identical. If the adsorbed protactinium species is thought of as an uncharged molecule held to other protactinium molecules or to solid surfaces by van der Waals forces, the relationship between adsorption and polymer formation becomes clear. At high ionic strength, the mobility of the adsorbable species is reduced, requiring either a greater surface area for adsorption or a higher concentration of protactinium for polymerization.

The controlled adsorption of such unlikely compounds as barium, strontium, and calcium chlorides based on their insolubility in non-polar solvents has been recently demonstrated.[10] Further study of the adsorptive tendencies of protactinium should shed additional light on the nature of protactinium species in aqueous solutions.

POLONIUM-208/POLONIUM-209

Macrochemistry In the continuing study of the isotopic mixture of polonium-208 and polonium-209, x-ray diffraction patterns employing strictly monochromatic radiation from a doubly bent lithium fluoride crystal have been obtained. The use of monochromatic radiation eliminates the parasitic wavelengths that contribute to the undesirable background. Microphotometer intensity curves of the x-ray diffraction patterns have been completed; consequently, the intensity curves have been placed on a relative basis which is necessary to compute the electron distribution curve on an absolute basis.

[9] J. G. Moore and R. H. Rainey, U.S.A.E.C. Report TID-7675, p. 16 (February, 1964).

[9] C. J. Hardy and D. Scargill, U.S.A.E.C. Report TID-7675, p. 1 (February, 1964).

[10] H. W. Kirby, "Residue Adsorption II. Separation of Barium-140 and Lanthanum-140 by Reverse Order Desorption", submitted for publication in *J. Inorg. & Nuclear Chem.*

Preliminary radial distribution curves on a relative basis have been calculated for polonium employing the relation:

$$r \sum_m K_m [g_m(r) - g_0] \cdot \sum_j [\exp(-\alpha S_j^2)] \sin 2\pi(r\, d_j)$$

with the temperature or convergence factor $exp(-aS^2_{j\,max})$ equal to 0.1, the other terms being defined in earlier reports.

In Figure 3 is depicted the relative radial distribution curve versus the interatomic distance for Po^{208}/Po^{209}. The peak at 3.5A is attributed to the Po-Po interatomic distance, which is in good conformity with the sum of Pauling's metallic radii of 3.52A. It has been established that α-polonium metal exists in the simple cubic structure, that is, with polonium atoms only at the corners of a cube. In this configuration each polonium atom is surrounded by six other polonium atoms in an octahedral configuration; the Po-Po interatomic edge distance should occur at $\sqrt{2}$ times the center-to-apex distance. In Figure 3 the Po-Po edge distance is at 4.9A which is in good agreement with the theoretical distance of 4.95A. The radial distribution curve also exhibits a Po-Po interaction at 6.8A, which is the distance between two polonium atoms in an adjacent unit cell.

More definitive and detailed structural analyses are presently being pursued by determining the number of nearest neighbors, both for the alpha and the beta phases.

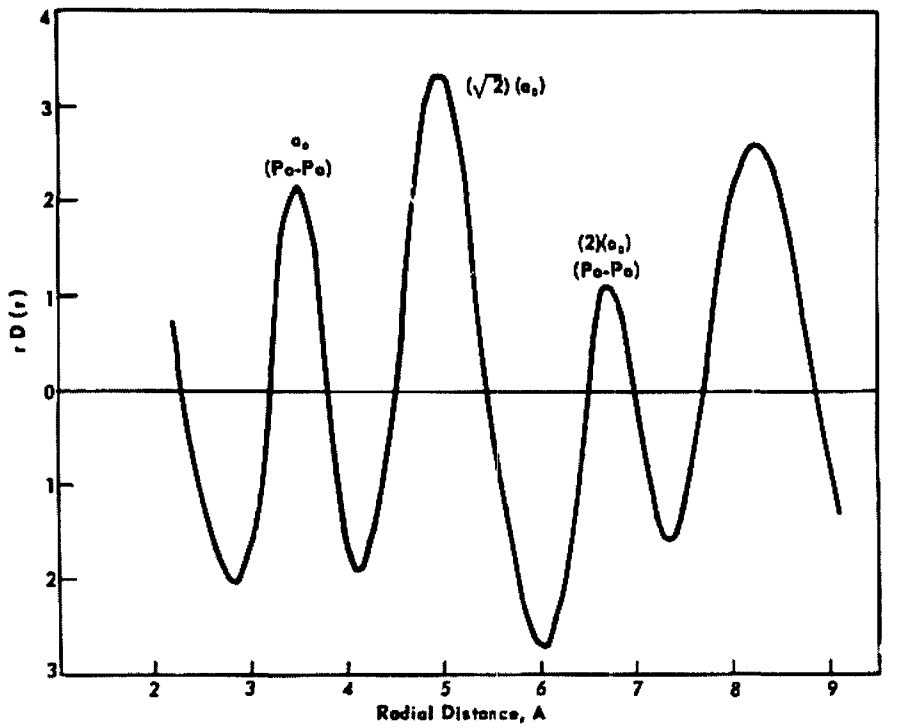

Figure 3. *Radial Distribution Curve for Polonium-208/Polonium-209*

ISOTOPE SEPARATION AND PURIFICATION

Under the sponsorship of the Division of Research, Mound Laboratory is responsible for furnishing material to be used in the physical sciences to further the progress of science and technology in the public interest. Purified helium-3 and isotopes of all other noble gases as well as carbon-13 are available for distribution. After recovery, purification and concentration, these isotopes are furnished to installations for research programs in the physical sciences. Methods of separation and purification are being studied.

CARBON-13

Thermal Diffusion The desired operating holdup of $C^{13}H_4$ was accumulated in the 12-column, 8-stage methane thermal diffusion system following a complete loss in August, 1964. Withdrawal of product was resumed at the rate of 2 cc per hour on December 2, 1964. The material being withdrawn from the cascade is methane of greater than 98% purity with a mass-17 enrichment of 98%. Recent performance of the cascade is depicted in Figure 4.

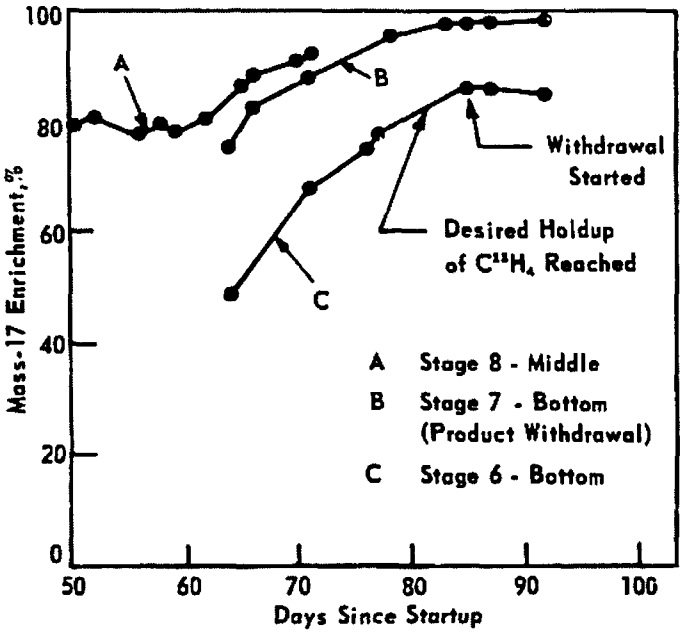

Figure 4. *Performance of the Methane Thermal Diffusion Cascade*

The operating holdup was accumulated over a period of 80 days. Small losses and down time from equipment failures were responsible for approximately 30 of the days; therefore, in the absence of such incidents the time to reach steady operation should be 50 days or less.

The performance of the cascade was improved and the time constant was decreased by dropping the operating pressure of Stages 3 through 8 from 740 to 560 torr. The drop in pressure increased the effective length of the cascade by 25%, and the operating holdup was reduced by more than 25%. Theoretical performance calculations for this arrangement have not yet been made.

In two r s 19.23 grams of BaC O, were prepared from the inventory of enriched methane. The material produced was at 92" enrichment in carbon-13 and contained 1.16 grams of carbon-13. The capacit of the conversion system has been increased up to 0.7 gram of carbon-13 can now be converted to barium carbonate in a single run.

Chemical Exchange Impr d techniques in the operation of the carbon dioxide-monoethanolamine chemical exchange apparatus increased the separation factor for carbon-13 from 1.10 to 1.20 for comparable reaction times. The separation factor of 1.20 represents a value corresponding to about 20% of the time required to reach equilibrium. Evidence was found that carbon dioxide is still present in the dissociated amine solution which is recirculated through the system. Increased decomposer temperatures indicate that decomposition was not complete.

HELIUM

A new charcoal trap in a cylindrical shape instead of a coil is being prepared for tritium removal experiments. The second experimental run on the charcoal trap in the coil shape showed no reduction of tritium from an initial concentration of 10^{-7}%. This was insufficient to meet our specification of 2×10^{-10}%. The trap had been evacuated and heated for degassing. The new style trap is expected to allow better degassing of the charcoal bed through improved conductance.

NEON

The 96-foot, 4-column, 4-stage cascade for the enrichment of the neon isotopes was started with gas containing neon-21 enriched to about 2%. The total amount of neon-21 in the system was approximately 600 cc. After 5 days the neon-21 peak reached a concentration of 19%.

The static neon-21 profile is shown in Figure 5.

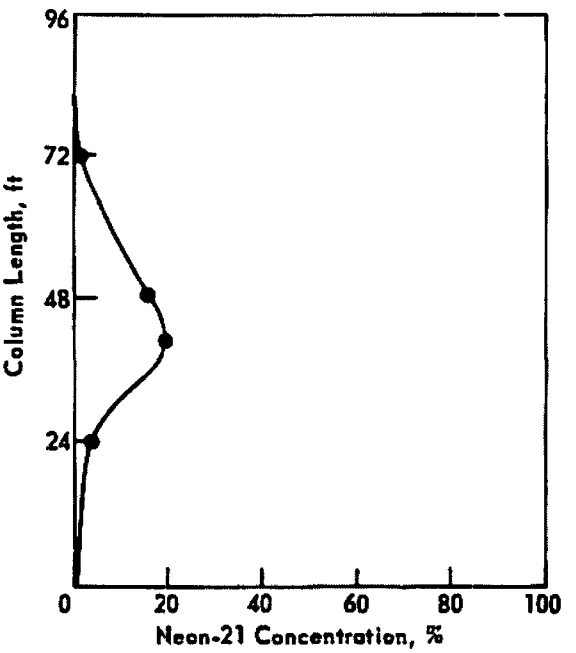

Figure 5. *Neon-21 Profile in the 96-Foot Thermal Diffusion Column After Running Under Static Conditions for 5 Days*

ARGON

In a four-stage cascade system, draw-off of argon-36 with a concentration of greater than 99.98% from the top of the fourth stage at the rate of 1.8 milliliters per hour has allowed a slow decrease of the concentration at the bottom of the last stage to 99.26% argon-36. At the same time the concentration of argon-38 in the bottom of the third stage has increased to 9.0%. Figure 6 shows the change in argon-38 concentration at the bottom of the third stage over a period of about two months.

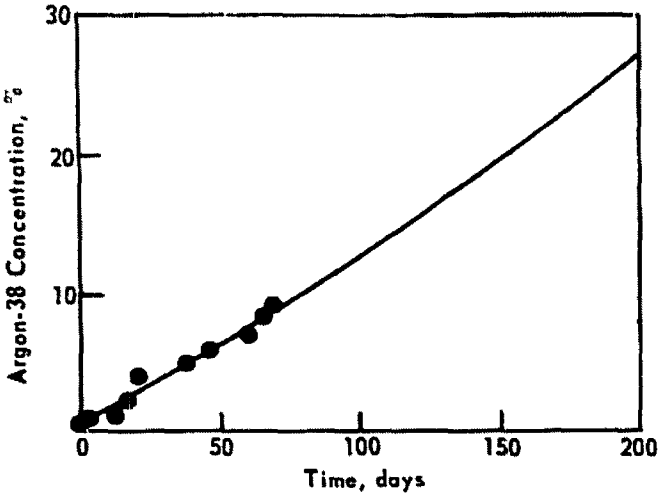

Figure 6. *Projected Buildup at the Bottom of the Third Stage of a Four-Stage Cascade*

KRYPTON

A two-column, two-stage cascade system is being used to enrich krypton-84 and -86. A draw-off of about 12 cc per hour from the bottom with a reservoir at the other end was started. The draw-off concentration has dropped over a period of time and has depleted the reservoir concentration to 14% krypton-86. Initially the draw-off concentration was about 35% krypton-86, and it has averaged about 28%. With this 28% krypton-86 as a starting material for the succeeding stages, it is estimated the three additional stages or passes will bring the concentration to over 90%, based on calculations summarized in Table 5.

Table 5

SUMMARY OF CALCULATIONS FOR 3-STAGE ENRICHMENT OF KRYPTON-86 TO 90% , STARTING WITH 28% KRYPTON-86

	Stage 1	Stage 2	Stage 3
Gas Volume, liters			
Beginning of Stage	57	16.83	4.59
Product	16.83	4.59	1
Product Flow, ml/hr	20	20	15
Number of Runs per Stage	3	3	2
Time per Run, hours	280	76	67
Column Pressure, torr			
Beginning of Run	330	330	330
End of Run	291	292	289
Kr-86 Concentration, %			
Beginning of First Run	28	46	68
Beginning of Last Run	23	41	65
Product	46	68	92

An independent krypton problem is the preparation of a quantity of krypton having a very low concentration of krypton-85. Krypton 85 is a radioactive isotope with about a 10-year half-life and is a fission product. Prior to the advent of nuclear reactors and weapons testing there was no detectable krypton-85 in the atmosphere, but since about 1950 there has been a steady increase in the amount of krypton-85 in the atmosphere. Although the concentration of krypton-85 in total krypton is quite small (approximately 10^{-11}% at present) there are some applications where even this small concentration cannot be tolerated. Consequently, Mound Laboratory will use thermal diffusion to produce krypton in which the krypton-85 content has been reduced to an acceptable level.

The krypton-85 in natural krypton will be reduced to a concentration of about 10^{-14}%. With present counting techniques a concentration lower than about 10^{-13}% cannot be measured. The product concentration can be calculated, however, if the feed concentration and the separation factor of the system are known. Some calculations of the product concentration have been performed for an idealized system consisting of a single thermal diffusion column of negligible volume with a 50-liter reservoir at the top of the column and a 2950-liter reservoir at the bottom.

The results of these calculations are presented in Figures 7, 8, and 9. In Figures 7 and 8, the concentration in the product (i.e., the top reservoir) of each of the stable isotopes of krypton is plotted as a function of the reduction in krypton-85 concentration. The reduction in krypton-85 concentration, the "reduction factor," is defined as the feed concentration of krypton-85 divided by the product concentration. By measuring the feed concentration of krypton-85 and the product concentration of one of the stable isotopes, the product concentration of the krypton-85 can be found from these curves. The concentration of the krypton-80 is very sensitive to the reduction factor, and by determining this concentration by means of mass spectrometry the reduction factor could be determined to within 2%.

The curves in Figures 7 and 8 are independent of the separation factor. The length of column necessary to obtain a given reduction factor is shown in Figure 9. The required length is proportional to the natural logarithm of the separation factor. The column lengths given in Figure 9 are for a column in which the ratio of the column transport constants, H/K, is equal to 7.76×10^{-3}. H and K were calculated for the isotope pair 84-86. The length of any column, L_x, with column constants $(H/K)_x$ may be obtained from a simple proportionality:

$$L_x = \frac{7.76 \times 10^{-3}}{(H/K)_x} L_e$$

where L_e is the length obtained from Figure 8.

In Table 6 the length of column necessary to reduce the krypton-85 content by a factor of 300 is given for columns having a hot-wall diameter of 5/16 inch and several cold-wall diameters. This is the reduction factor required to reduce the krypton-85 concentration to 10^{-14}% in krypton gas that was collected from the atmosphere in 1954. All the columns in this table have the following common characteristics: hot wall diameter 5/16 inch (nominal) - 0.315 inch (actual); $T_1 = 300$°K; $T_2 = 1023$°K. The cold-wall diameter of the column is given in the first two columns of the table. The length of column is given for two values of

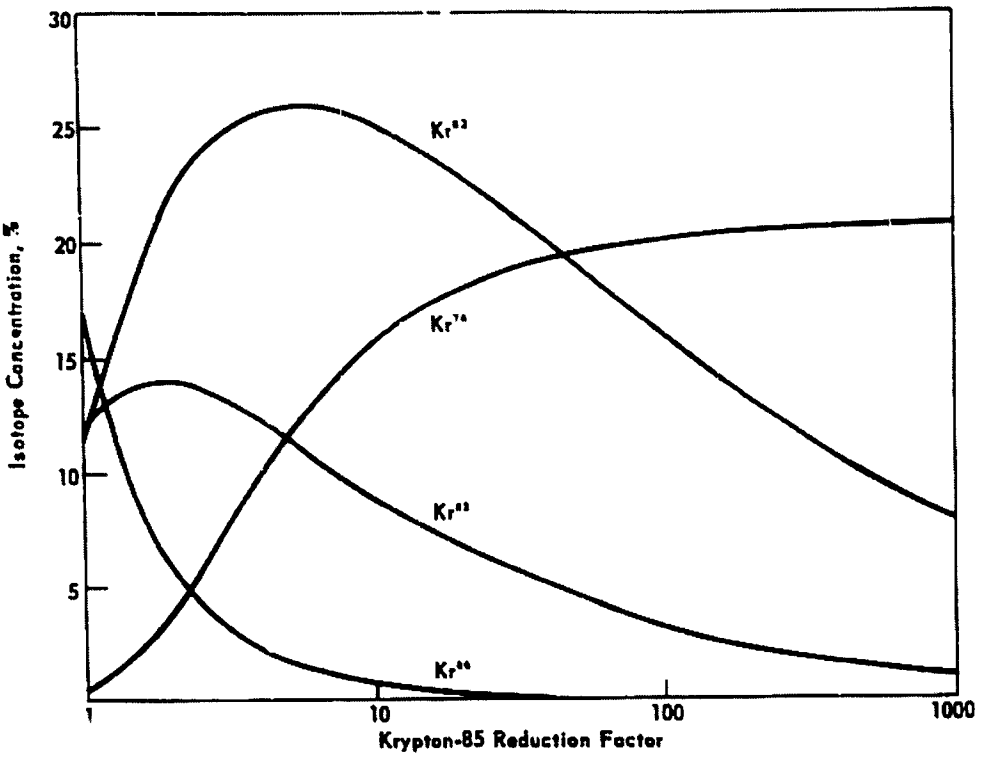

Figure 7. *Concentration of Four Stable Isotopes of Krypton as a Function of Reduction of Krypton-85 Concentration.*

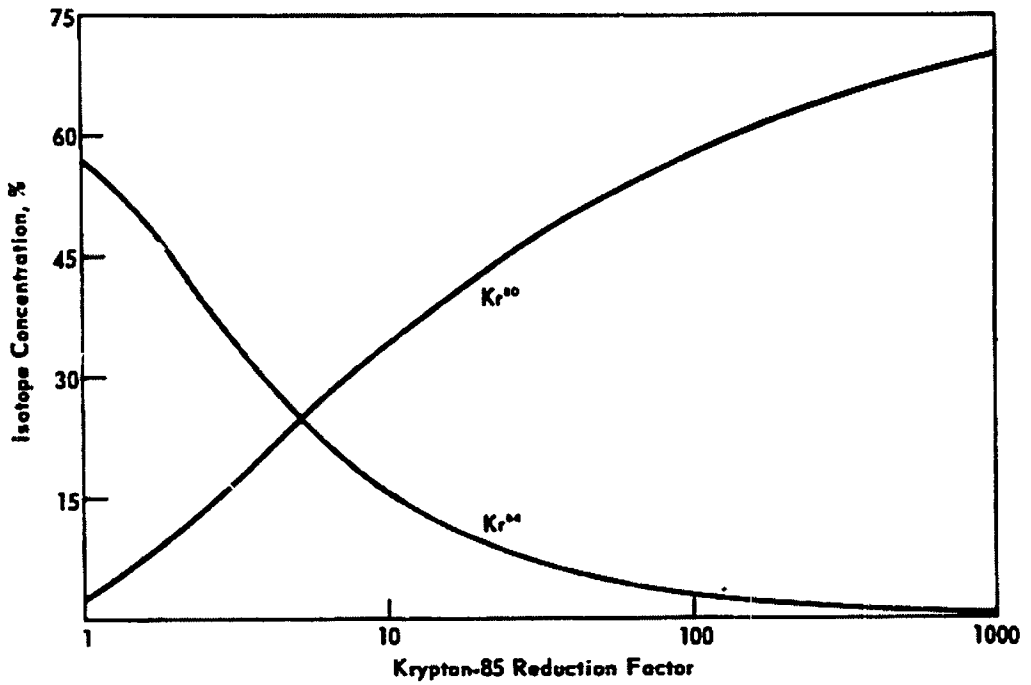

Figure 8. *Concentration of Two Stable Isotopes of Krypton as a Function of Reduction of Krypton-85 Concentration.*

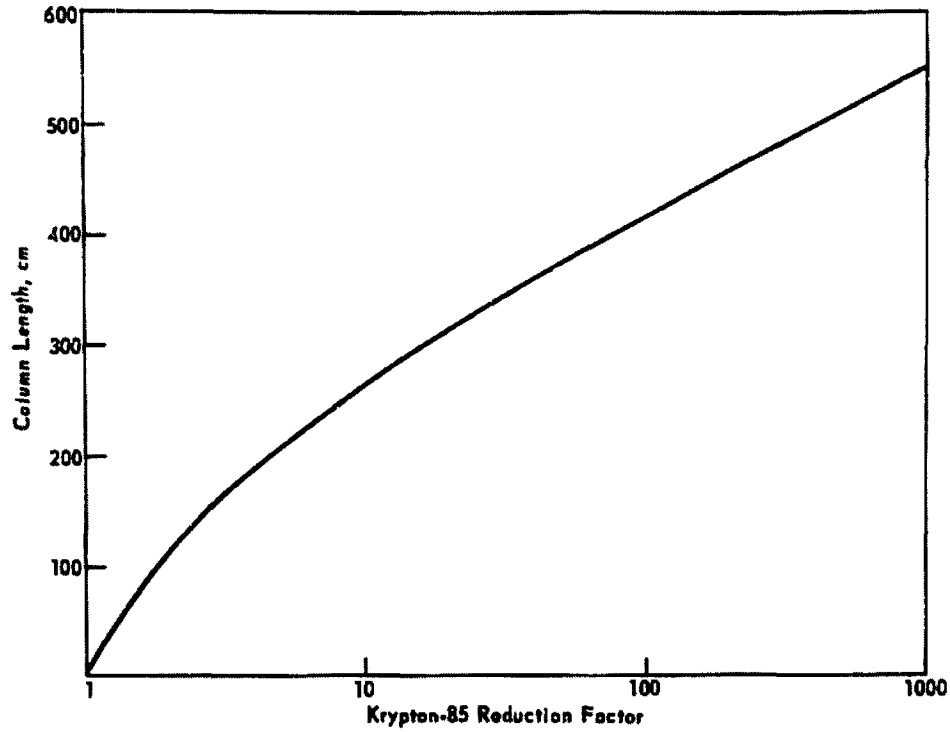

Figure 9. *Column Length Required to Obtain a Given Reduction in Krypton-85 Concentration*

K_c/K_d, which corresponds to two different operating pressures, for each cold-wall diameter. The conversion factor is the quantity $7.76 \times 10^{-3}/(H/K)_x$. The transport coefficient H given in the table is with respect to the separation of krypton-84 and -86. The transport coefficient with respect to any other two isotopes can be obtained from the relation

$$H_{i,j} = 85\left(\frac{M_j - M_i}{M_i + M_j}\right)(H_{84,86})$$

The ratio of the volume of the column to the volume of the top reservoir, which in all cases equals 50 liters STP , is given in the last column of the table. These figures show that the volume of the column would be small compared to the volume of the top reservoir, as was assumed in the calculations.

According to the figures in the table, a few 12-foot columns could reduce the krypton-85 concentration by a factor of 300. This is the reduction that would be obtained when the system reached equilibrium. However, if only a few columns are connected in series, it would take an extremely long time for the system to reach equilibrium. An order-of-magnitude estimate of the time required for the krypton-85 to reach its equilibrium concentration can be obtained by calculating the initial transport of krypton-85, which is given by

$$T^0_{85} \quad H_{85,86}X_{85} - X_{85}\sum_j H_{j,86}X_j$$

Table 6

THERMAL DIFFUSION DATA FOR KRYPTON-85 REDUCTION EQUIPMENT

Cold Wall Diameter (in.)							
Nominal	Actual	K_c/K_d	Pressure (atm)	Length (cm)	Conversion Factor	$H_{84,86}$ (g/sec)	Volume Ratio
9/16	0.568	1	1.28	510	1.05	1.06×10^{-3}	0.015
		10	2.28	890	1.83	3.34×10^{-3}	0.046
10/16	0.631	1	0.904	635	1.31	1.12×10^{-3}	0.017
		10	1.61	1105	2.28	3.53×10^{-3}	0.054
11/16	0.693	1	0.678	760	1.57	1.18×10^{-3}	0.020
		10	1.21	1325	2.73	3.72×10^{-3}	0.062
12/16	0.756	1	0.531	890	1.83	1.23×10^{-3}	0.023
		10	0.944	1545	3.19	3.90×10^{-3}	0.070

In this equation the X's are the feed concentrations which for the six stable isotopes are:

Mass No.	78	80	82	83	84	86
Concentration (%)	0.35	2.27	11.56	11.55	56.90	17.37

For a 5/16-inch x 9/16-inch column operating at $K_c/K_d = 10$ the initial transport is

$$T^o_{ss} = 1.63X_{ss} \text{ g/day}$$

The total amount of krypton-85 that must be transported out of the top reservoir to reduce the concentration by 300 is $189X_{ss}$ grams.

At the initial rate of transport it would take 116 days to transport this amount. It is apparent that in order to obtain a reasonable equilibrium time several columns in parallel must be used. If ten columns in parallel were used, it would take 11.6 days at the initial rate to transport the total amount of krypton-85. Of course, the rate of transport decreases with time, so it would take much longer than 12 days for the krypton-85 to reach its equilibrium concentration. A reasonable estimate for the equilibrium time would be 150 days.

In a multicomponent system all the components do not reach their equilibrium value at the same time. For example, in the case considered above it would take 85 days at the initial rate of transport to transport the total amount of krypton-80 into the top reservoir. Thus, the krypton-85 would attain its equilibrium value much sooner than the krypton-80. Consequently, the method of determining the reduction in krypton-85 concentration outlined above only applies to a column at equilibrium. It is possible to design a system of columns so that the equilibrium times of the krypton-80 and -85 are approximately equal. Although such a system would not be very efficient for the reduction of the krypton-85 concentration, the waste material from such a system would be valuable. Since it would be depleted in krypton-78 and -80 it could be used as feed material in a system to enrich krypton-82.

XENON

Thermal Diffusion The six-stage cascaded thermal diffusion system with two swing units was started with fresh fission xenon after a pressure upset due to stalling of the timer gear. With fresh feed, the decrease in xenon-131 concentration at the product end has been slow. Presently it is 1.0% xenon-131.

Gas Chromatography Xenon obtained as a reactor off-gas contains krypton-85 as an impurity. This impurity is removed chromatographically. An experimental chromatograph was built to study the parameters that affect separation. A xenon processing chromatograph was built according to a design based on information gathered with the experimental unit.

A series of separations on the experimental unit was made using argon as the carrier gas. The runs were made using temperature programming. The initial temperature is approximately -106 C; it remains in this region until the krypton-85 reaches its peak concentration. Then the column is warmed up at a rate of about 3°C min until the temperature is about -45°C, when the rapid warming is ceased. When the xenon peak emerges from the column the traps are switched and the xenon is collected while the column is purged at a high temperature. When argon is used as carrier gas, liquid argon is used around the xenon trap to avoid freezing argon in the trap.

The results of these separations are shown in Table 7. Argon seems to give a higher cleanup (ratio of krypton-85 concentration of feed to xenon trap recovery) than does nitrogen. It was expected that the heavier argon would be more efficient since the effect was observed in going from helium to nitrogen and has also been reported by others. Unfortunately, with liquid argon around the trap some xenon is lost (about 5% or less). The feed totals about 1000 cc.

Table 7

KRYPTON-85 CLEANUP BY GAS CHROMATOGRAPHY

Separation Number	Carrier Gas	Flow Rate (l/min)	Recovery (cc, STP)	Time for Run (min)	Cleanup
1	Ar	2.61	1024	117	5,110
2	Ar	3.4	901	126	13,650
3	Ar	3.4	984	108	16,020
4	Ar	4.1	952	106	20,760
5	Ar	3.4	975	119	16,280
6	N_2	4.5	965	82	12,700

Where argon is the carrier gas, higher cleanups are obtained when larger flow rates are used.

In actual practice the use of argon is not recommended as a carrier gas. A 5% loss of xenon in each separation cannot be tolerated. Further, any argon that remained in the product would be difficult to remove.

THERMAL DIFFUSION RESEARCH

Molecular Beam Scattering The single-beam apparatus has been constructed, assembled and aligned inside a laboratory bell jar vacuum chamber.

Some preliminary runs were made with argon feed gas at room temperature to determine the operational capability of the opposed NRC ionization gauge network. It was found that, with this chamber and pump arrangement, a 1-torr source pressure is unobtainable without increasing the chamber residual pressure to the point where the beam is attenuated by residual scattering to the extent that the detector system is rendered insensitive to the beam. The capacity of the diffusion pump is too low (1000 l/sec at 10^{-4} torr) to remove the scattered particles from all three sections of the beam collimation fixture. Ideally, each section should have its own pumping system to maintain as low a residual pressure in each section as possible.

Since the desired beam intensity could not be obtained, the lower limit of the equivalent beam pressure that this type of detection system was capable of sensing was to be determined. In the first run the beam was seen by the detector at a source pressure of 10^{-3} torr. At this pressure the beam intensity at the detector was decreased about three orders of magnitude (to 5×10^{-11} mole/sec) from the original proposed design. This gives an apparent relative detection sensitivity of a change of 1×10^{-6} torr in a residual pressure of 1×10^{-3} torr, or 0.1%.

The pressure difference between the beam and residual gauge tubes was monitored on a Honeywell Electronik-17 dual pen recorder along with the source pressure.

Since the NRC ionization control outputs could not be directly connected in an opposed manner due to mismatching of the two circuits, the recorder input was taken between the plates of the amplifier tubes in each control unit. The first run was made without attempt to match the two control units electronically. Thus, circuit changes due to pressure variations did not maintain a consistent relationship to each output and the readings obtained were incoherent, showing only relative beam pressure changes.

The instruments have since been modified to make them electronically similar. Figure 10 shows a corresponding pair of traces of the detector system relative response to various source pressure surges from 10^{-3} to 10^{-1} torr. The residual gauge detects a greater increase initially as shown by a negative swing in the detector reading; however, as the beam gauge approaches equilibrium about two seconds later the detector reading swings positive, showing the beam pressure as a difference reading between the two gauges. The detector response readings are being calibrated and controlled tests will be made over the range of detectability.

Transport Coefficients Seven thermal diffusion columns are being used for experimental determination of column transport coefficients. Dimensions and current operating temperatures of these columns are given in Table 8.

Two sets of measurements are required to determine the coefficients H', K_c' and K_d in the differential equation for isotope transport in a binary mixture:

$$\tau = H' p^2 c(1-c) - (K_c' p^4 + K_d) \frac{dc}{dz}$$

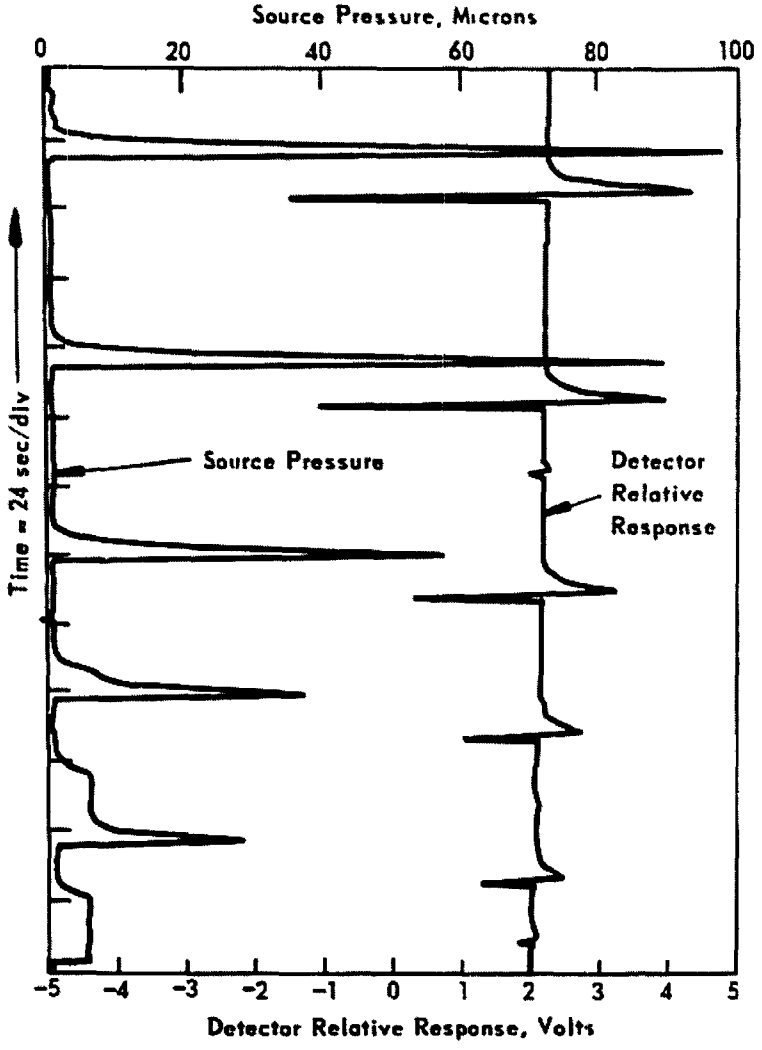

Figure 10. *Detector Response Vs. Source Pressure*

where r is the rate of transport of the desired isotope toward the positive end of the column, p is the pressure, c is the fraction of one of the isotopes, and z is the vertical coordinate. The required experiments are (1) measurement of static separation factor as a function of pressure, and (2) measurement of separation as a function of flow rate.

Measurements for methane in Column E6 (see Table 8) were completed, and the data were processed to obtain transport coefficients for a wire temperature of 450°C; the coefficients for a wire temperature of 300°C were determined and reported earlier.[11] Both sets of transport coefficients are given in Table 9 along with values predicted from theory with Lennard-Jones shape factors.[12] An accurate value of α, the

[11]MLM-1216, p. 13.

[12]B. B. McInteer and M. J. Reisfeld, LAMS 2517, (1961).

thermal diffusion factor at the cold wall temperature, is not available; therefore, at 300°C a value was calculated from the experimentally measured value of H' and the theoretical value of (H'/α_o):

$$\alpha_o \quad \frac{H'_{exp}}{(H'/\alpha_o)_{theory}}$$

As reported earlier[11], a value of 0.0057 was found for α_0 at 288°K. This α_0 value was used in the theoretical calculation of H' for a 450°C wire temperature.

Table 8

DIMENSIONS AND OPERATING CONDITIONS OF THERMAL DIFFUSION COLUMNS FOR DETERMINATION OF COLUMN TRANSPORT COEFFICIENTS

Column	Length (cm)	Cold Wall Radius (cm)	Hot Wall Radius (cm)	Cold Wall Temp. (°C)	Hot Wall Temp. (°C)	Gas
E1	365.8	1.27	0.0794	15	800	Ne
E2	365.8	1.60	0.0794	15	800	Ne
E3	365.8	1.90	0.0794	15	800	He
E4	365.8	2.05	0.0794	15	800	He
E5	182.9	0.945	0.0794	15	800	Ne
E6	731.5	0.953	0.0794	15	300, 450	CH_4
E7	365.8	0.721	0.400	30	400	CH_4

Table 9

COLUMN TRANSPORT COEFFICIENTS FOR METHANE IN COLUMN E6

	T_2 = 300°C	T_2 = 450°C
$10^3\ H'$ (measured)	1.36	2.08
$10^3\ H'$ (theory)	(1.36)[a]	2.08
$10^2\ K'_c$ (measured)	2.19	1.74
$10^2\ K'_c$ (theory)	2.11	2.01
$10^4\ K'_d$ (measured)	4.78	5.75
$10^4\ K'_d$ (theory)	5.02	5.55

[a]The measured value of H' at 300°C was used to calculate α_0 for the theoretical calculation.

The agreement between theory and experiment is quite satisfactory. The maximum deviation is 14% for K'_c at 450°C. This deviation is in an unexpected direction since the predicted value of K'_c is larger than the measured value. Parasitic circulation effects in the column would tend to cause deviations in the opposite direction. In any case it is doubtful that the difference is greater than the expected precision of the experiments.

In other experiments static separations were measured for methane in Column E7. Values of H/K vs. pressure for these experiments are plotted in Figure 11 along with values calculated from theory using Lennard-Jones shape factors. In the theoretical calculation an α_0 of 0.0060 was used. At the cold-wall temperature of 303°K this value is consistent with the value of 0.0057 used above for a 288 K cold-wall temperature. Columns similar in design to Column E7 are to be used in a planned addition to the methane thermal diffusion cascade for carbon-13 separation.

The static separation as a function of pressure was obtained for helium in Column E4. A plot of this data when helium-3 is 50% of the total helium is shown in Figure 12. Also depicted in Figure 12 are theoretical values of H/K calculated from Lennard-Jones shape factors. An α_0 value of 0.0635, interpolated from Watson's data,[13] was used in the calculation.

Because of the high separation between the helium isotopes, essentially 100% helium-3 accumulates at the top of the column and 100% helium-4 at the bottom. Helium-3 and helium-4 have different properties; therefore the thermal diffusion factor, α, the viscosity, η, and the density, ρ, vary along the column. Since the separation factor is a function of α, η and ρ, it was necessary to find H/K as a function of the helium-3 concentration along the length of the column. For each pressure plotted, four gas samples were taken along the column and analyzed for the isotopic ratios. From these data H/K was calculated and plotted versus helium-3 concentration along the length of the column. Typical results for measured and predicted values of H/K versus composition are given in Figure 13 for Column E4 at 1072 torr. From a series of plots similar to that of Figure 13 values of H/K for 50% helium-3 were picked off and plotted versus pressure to obtain Figure 12.

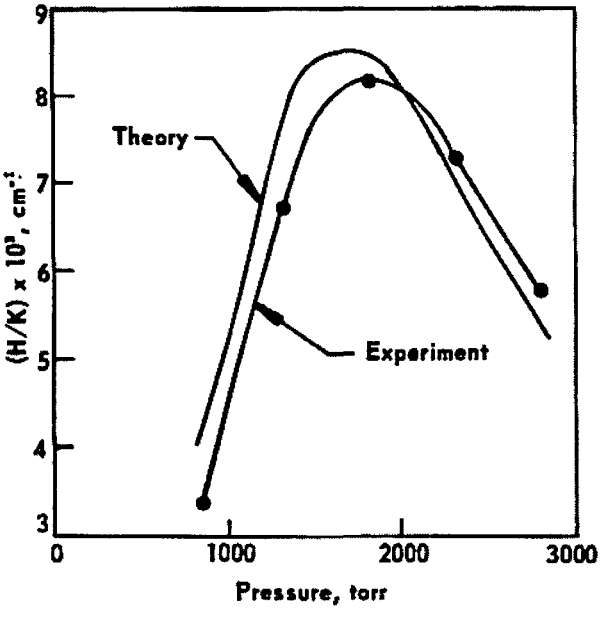

Figure 11. *H/K Vs. Pressure for Methane in Column E7*

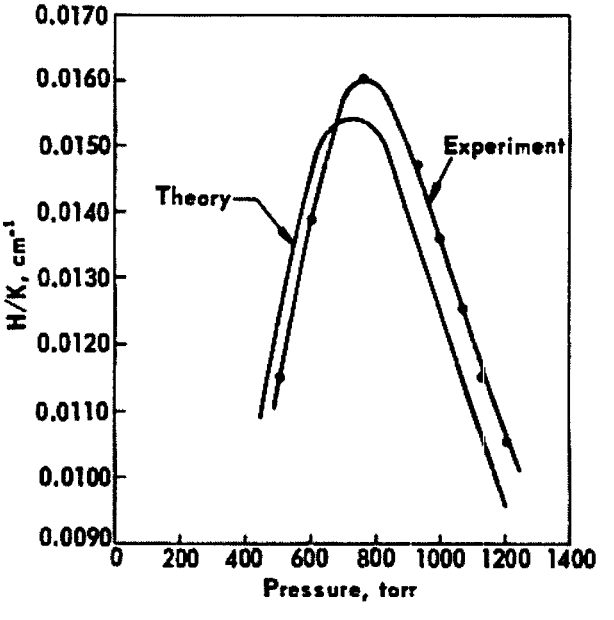

Figure 12. *Static Separation Factor Vs. Pressure for Helium-3 and -4 in Column E4*

[13] W. W. Watson, et al., *Z. Naturforschg.*, 18A, 242 (1963).

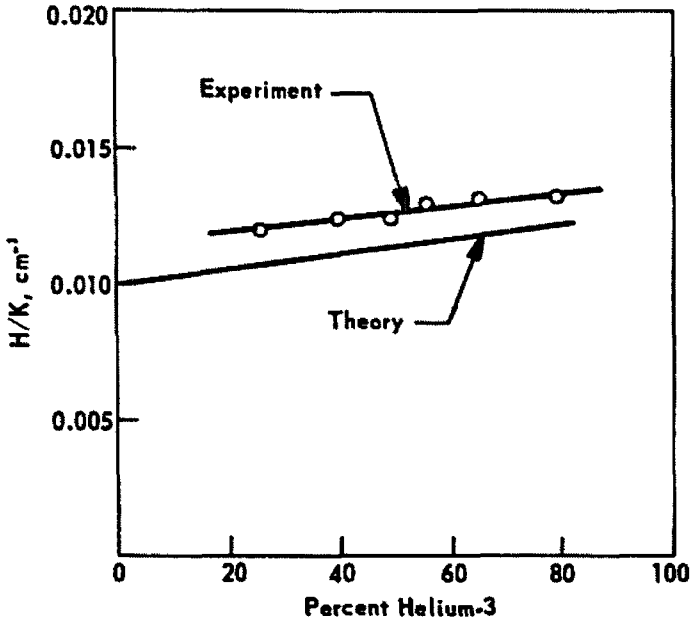

Figure 13. *H/K Vs. Composition for Helium in Column E4*

HELIUM RESEARCH

Vapor Pressure Thermometry A single run of three days duration was made on the vapor pressure thermometry apparatus using only unsaturated helium-4 in the bulb and liquid helium-4 in the inner and outer cooling baths. Data were taken for the 1/8, 1/16, and 1/32-inch tubes versus the 1/4-inch tube at two constant cold temperatures, 4.2° and 2.0°K.

The technique was both simple and rapid. The inner bath was maintained at one of the cold temperatures while the pressure in the bulb was measured through the nominal 1/4-inch tube. Simultaneously, the pressure difference between the warm ends of the 1/4-inch tube and one of the small tubes, all of which are directly open to the bulb, was measured. The bulb pressure was changed by pumping out or admitting gas. The warm end pressure in the 1/4-inch tube is designated as $p_{w1/4}$ and represents the true pressure, p_c, in the cold bulb plus the thermomolecular pressure difference for a 1/4-inch tube, $\Delta p_{1/4}$, at the existing conditions.

That is,

$$p_{w1/4} = p_c + \Delta p_{1/4}$$

and similarly for the other tube sizes:

$$p_{wd} = p_c + \Delta p_d$$

where the subscript d designates the tube diameter. The differential pressure between two tubes d_1 and d_2 at the warm ends is

$$\Delta p_{d_1 - d_2} = p_{w d_1} - p_{w d_2}$$

$$= (p_c + \Delta p_{d_1}) - (p_c + \Delta p_{d_2}) = \Delta p_{d_1} - \Delta p_{d_2}$$

This experiment was carried out in order to determine if previous discrepancies between Mound Laboratory observations and the Weber-Schmidt predictions as confirmed at Los Alamos Scientific Laboratory could possibly be related to the fact that the Mound Laboratory measurements were done mostly below 1.6°K whereas the Weber-Schmidt and the Los Alamos work was at 1.9°K and above. This possibility is suggested by considerations of the temperature dependence of the viscosity.

In the present situation it is useful to compare a plot of the observed values of $p_{w\frac{1}{4}}$ as $\Delta(\Delta p_{d-\frac{1}{4}})$ with the predictions of the Weber-Schmidt equation and with previous data taken at Mound Laboratory. Such a plot is shown in Figure 14. The solid curves represent the Weber-Schmidt predictions for the indicated nominal tube sizes.

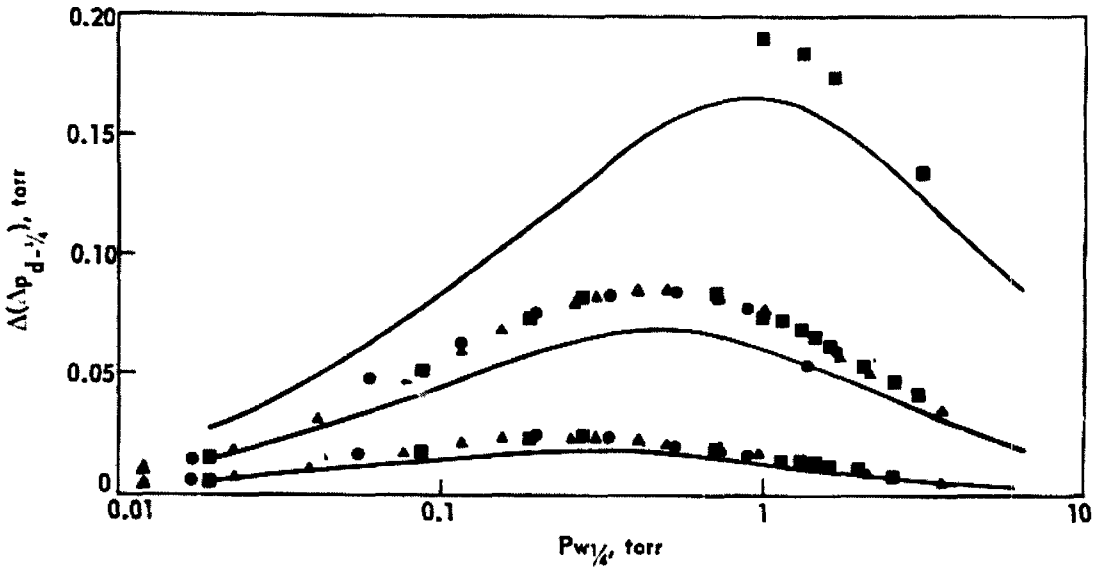

Figure 14. *Comparison of Differential Pressure Data*

In the calculations, tube inside radii of 0.281900 cm (1/4 inch nominal), 0.133350 cm (1/8 inch nominal), 0.054610 cm (1/16 inch nominal), and 0.024450 cm (1/32 inch nominal) were used. The warm temperature was varied according to the vapor pressure relation of p_c on the 1958 Helium-4 Scale.

The data points (squares) were taken with stainless steel tubes of inside radii of 0.29, 0.14, 0.055, and 0.0271 cm; T_c was 4.22± 0.02°K and T_w was 300.3 ± 0.7°K. The points were taken as the bulb pressure was reduced in steps.

Other data points (circles) were taken with the same tubes; T_c was 4.22 ± 0.02°K and T_w was 299.0 ± 1.4°K. The points were taken as the bulb pressure was increased in steps.

Data points represented by triangles were also taken with the same tubes when T_c was 2.00 ± 0.02°K and T_w was 298.5 ± .4°K. The points were taken as the bulb pressure was reduced in steps.

Theoretically T_w should be controlled within closer limits, but the data appear to be sufficiently smooth and reproducible for the present purposes. General comments on the data are given below:

1. The four points for the 1/32-inch tube coincide with previous Mound Laboratory data taken on a different 1/32-inch tube. An entirely different experimental apparatus was used, including different pressure measuring devices.

2. The deviations of the points from the Weber-Schmidt predictions have the same general shape for all three tubes with values at the maximum $\Delta(\Delta p)$ of 26.3, 24.1 and 17.5 for the 1/8, 1/16 and 1/32-inch tubes, respectively.

3. At the low-pressure end of the $\log p_{RT_4}$ axis, where the experimental matter is most evident, a detailed comparison of individual point spacings for the 1/8 and 1/16-inch tubes strongly suggests small systematic instrumental errors.

4. The data converge with the Weber-Schmidt calculations both at the high and low-pressure ends (i.e., the boundary conditions which have a firm theoretical basis are satisfied).

General conclusions may be drawn from the data:

1. The insensitivity to T_c at high and intermediate pressures as predicted by Weber-Schmidt is clearly shown by the coincidence of the 4.2°K and 2.0°K data points.

2. The discrepancies between the present and previous Mound Laboratory data as opposed to the Weber-Schmidt predictions are definitely not directly or wholly related to the particular working temperatures, T_c, in the various experiments.

3. These data, which were obtained for unsaturated gas, do not agree with the single previous Mound Laboratory saturated gas data on the low-pressure side of the maximum $\Delta(\Delta p)$. At the peak and at higher pressures the agreement is good. Therefore, it is of prime interest to check reproducibility on the experimentally difficult saturated data below the peak.

4. If the observed deviations are real, they represent non-negligible adjustments of accepted thermomolecular pressure corrections for helium-4. For example, the present data when used for vapor pressure temperature determinations would shift calculated temperatures at 1°K by approximately 5 and 10 millidegrees for vapor pressure sensing tubes of 1/8- and 1/16-inch diameters, respectively, with the warm end at room temperature. By comparison, the uncertainty in the T-58 vapor pressure scale is reported to be ± 2 millidegrees.

The differential equation employed in the Weber-Schmidt[14] derivation of the expression for the thermomolecular pressure difference is as follows:

$$u = \sqrt{\frac{\pi}{2}}\sqrt{\frac{M}{RT}}\,\frac{\eta}{\rho}\,\frac{du}{dx_1} - \frac{3}{4}\,\frac{\eta}{\rho T}\,\frac{dT}{dx_2}$$

The variables represent the following quantities:

u = velocity of gas flow parallel to the wall
M = gram molecular weight
R = universal gas constant
T = absolute temperature
η = viscosity
ρ = density
x_1 = length coordinate perpendicular to wall
x_2 = length coordinate parallel to wall

Weber assumed that the equation above should reduce to Poiseuille flow in the absence of a temperature gradient. This assumption would be valid when the mean free path of the gas is short compared to the dimensions of the container. The results of this derivation were meshed with results derived in the Knudsen region to yield an equation for the thermomolecular pressure difference which is applicable over the entire pressure region. Meshing of the derivations required the use of empirical constants obtained from experiment. Furthermore, the viscosity was expressed as a simple power law (Sutherland model) which is now known to be considerably in error over large temperature spans and is particularly unsuited to predicting viscosities in the quantum region. In view of these assumptions it appears advisable to investigate the regions separately.

It will be assumed that the mean free path is small compared to the dimension of the tube, (i.e., $r_T >> \lambda$).

For laminar flow in a capillary, Poiseuille's Law is

$$\frac{du}{dr} = \frac{dp}{dl}\,\frac{r}{2\eta}$$

where u is the flow velocity, r the radial coordinate, p the pressure, l the length, and η the viscosity. The subscript o will be used to denote value of the variables at the boundary, or inner wall, of the capillary. The differential equation may be integrated to yield

$$u = \frac{1}{4\eta}\,\frac{dp}{dl}\,(r^2 + C)$$

For an experimental system with a capillary open to two reservoirs and the entire system in equilibrium, the net transport must be zero:

[14] S. Weber, *Leiden Comm.*, No. 718, 11-33 (1932).

$$1 \quad 0 \quad 2\pi\int_0^{r_0} ur\,dr$$

$$\frac{2\pi}{4\eta}\frac{dp}{dl}\int_0^{r_0}(r^2 + C)\,r\,dr$$

$$= \tfrac{1}{4}r_0^4 + \tfrac{1}{2}Cr_0^2$$

The constant of integration is found to be

$$C = -\tfrac{1}{2}r_0^2$$

Thus the velocity u_0 at the boundary may now be defined:

$$u_0 = \frac{1}{8\eta}\frac{dp}{dl}r_0^2$$

It is just the two quantities, u_0 and du_0/dr, defined above, which appear in the equation for the flow of gas at a wall if one has an infinitely large tube such that

$$\frac{du}{dx_1} \longrightarrow \frac{du_0}{dr}$$

Once again, it may be argued that this is valid if the mean free path is small compared to r_0. In addition the equation should be equivalent to Poiseuille's Law in the absence of a temperature gradient.

$$u_0 + \gamma\frac{du_0}{dr} = \frac{3}{4}\frac{\eta}{\rho T}\frac{dT}{dl}$$

where $\gamma = \sqrt{\frac{\pi}{2}}\sqrt{\frac{M}{RT}}\frac{\eta}{\rho}$. Substituting the expressions for u_0 and du_0/dr into this expression yields:

$$\frac{1}{8\eta}\left|\frac{dp}{dl}\right|r_0^2 + \gamma\left|\frac{r_0}{2\eta}\frac{dp}{dl}\right| = \frac{3}{4}\frac{\eta}{\rho T}\frac{dT}{dl}$$

and

$$\frac{dp}{dT} = \frac{3}{2}\frac{\eta^2}{\rho T}\left[\frac{1}{r_0^2 + 4\gamma r_0}\right]$$

In order to separate the variables, it is again necessary to invoke the assumption that $r_0 \gg \lambda$. The following reasoning shows that the term containing γ may be neglected compared to r_0^2. Since from simple kinetic theory,

$$\lambda = \frac{kT}{\xi p\pi\sigma^2} = A\frac{T}{p}$$

and

$$\nu \quad \sqrt{\frac{\pi}{2}}\sqrt{\frac{M}{RT}}\,\frac{\eta}{\rho} \qquad \sqrt{\frac{\pi}{2}}\sqrt{\frac{R}{M}}\,\frac{\eta\sqrt{T}}{P} \qquad R\,\frac{\eta\sqrt{T}}{p}$$

since $\rho = nm = \frac{pM}{RT}$.

Now η is proportional to $\sqrt{T}$ in the first approximation, so γ is proportional to T/p, as is the mean free path. Hence one is justified in neglecting the term containing γ.

$$\frac{dp}{dT} = \frac{3}{2}\,\frac{\eta^2}{pTr_o^2}$$

or

$$pdp = \frac{3}{2}\,\frac{\eta^2 R}{M\gamma_o}\,dT$$

The left hand side may be integrated readily but the viscosity will not exhibit an exact $\sqrt{T}$ dependence, especially in the quantum regions. It is therefore desirable to leave the viscosity as an arbitrary function of temperature in order to complete the derivation.

$$\frac{1}{2}\,p^2\Big|_{p_{cold}}^{p_{hot}} = \frac{3}{2}\,\frac{R}{Mr_o^2}\int_{T_{cold}}^{T_{hot}} \eta^2(T)dT$$

If p_{cold} is assumed to be the vapor pressure, corresponding to the accepted helium scale, and which corresponds to the cold bulb temperature, then the pressure measured at the hot end of the tube will be

$$p_{hot} = \left[\frac{3R}{Mr_o^2}\int_{T_{cold}}^{T_{hot}} \eta^2(T)dT + p_{cold}^2\right]^{1/2}$$

ANALYTICAL AND INSTRUMENTATION

Methods of analyzing elements and compounds are being developed to support the programs at Mound Laboratory. These methods include instrumental techniques and standard wet methods.

NEPTUNIUM ANALYSIS

Optimum conditions for the separation of neptunium from plutonium have been determined. This will permit use of a spectrophotometric procedure in place of the time-consuming mass spectrographic method.

Table 10 presents the distribution coefficients for neptunium(IV) and (V) and plutonium(IV) between nitric acid media and tri-n-octylphosphine oxide (TOPO) dissolved in cyclohexane. The distribution coefficient E_a is the ratio of the alpha activity of each species - neptunium(IV) or (V) or plutonium(IV) - in the organic phase compared to the species in the aqueous phase. A value of E_a equal to 100 is equivalent to a recovery of greater than 99%.

Table 10

DISTRIBUTION COEFFICIENTS IN HNO_3

	E_a		
HNO_3 (*M*)	Np(IV)	Np(V)	Pu(IV)
0.15	14	0.01	100
0.30	30	0.015	--
0.50	180	0.020	--
0.75	250	0.02	--
1.0	300	0.02	150
2.0	122	0.04	200
4.0	--	0.56	400

The distribution coefficients for the extraction of thorium(IV) and uranium(VI) are not given in Table 10, but these values are equal to or greater than 100 at low nitrate concentrations. The table indicates that plutonium(IV), uranium(VI) and thorium(IV) can be extracted from 0.1*M* HNO_3 with TOPO, while neptunium(V) remains in the aqueous phase. The proper valences of the cations are obtained by boiling the solution with permanganate and then adding sodium nitrite, which destroys the permanganate and reduces plutonium(VI) to plutonium(IV) and neptunium(VI) to neptunium(V). The interfering cations are then extracted, leaving neptunium(V) in the aqueous phase.

An aliquot is taken from the aqueous phases and is adjusted to 1.0*M* HNO_3. Ferrous sulfamate is added to reduce neptunium(V) to neptunium(IV). Neptunium(IV) can be extracted with TOPO with 99% recovery. The neptunium content of the organic phase is measured spectrophotometrically. The colorimetric method has been described previously and involves the formation of the violet-colored neptunium-arsenazo complex in ethanol at pH 0-10. The absorbancy of this complex is proportional to the neptunium concentration.

All interfering cations are removed in the initial extraction step, so that only the anions sulfate and phosphate interfere through incomplete extraction of neptunium. However, these anions are not present in these materials, so the method is now ready for routine analyses.

COBALT ANALYSIS

A procedure for the determination of cobalt in plutonium metal was developed. Nitroso-naphthol forms a strongly colored complex with cobalt in citrate buffer at pH 3-4. This complex can be extracted with chloroform along with the excess nitroso-naphthol, which can be removed later by back-extraction with 5% NaOH. The absorbancy of the colored complex left in the organic phase can be measured by a spectrophotometer at 580 mμ. The absorbancy is proportional to the cobalt concentration up to 200 micrograms per 50 ml.

Plutonium(III) was found not to interfere with this determination when less than 10 mg of plutonium were present. Plutonium(III) is produced in citrate buffer by the addition of hydrogen peroxide. Two samples were analyzed and no detectable amounts of cobalt were found. Known amounts of cobalt were added to some of these unknown solutions and 100% recovery of this cobalt was obtained.

ANALYSIS OF ENRICHED URANIUM-234 FOR COMPARISON PURPOSES

A sample of enriched uranium-234 was analyzed by proportional counting according to method 2.406 of TID-7029[11]. When the counting chamber was purged for 45 seconds with P-10 gas (before the first of two 5-minute counts), a significant decrease in counting rate with elapsed time was observed. Apparently something on the slide mount was changing the characteristics of the counting gas. Constant purging of the chamber during counting eliminated the difficulty and a uranium-234 concentration of 1.51 wt % was indicated. The same slide mounts counted with a single 45-second purge indicated 1.68 wt % uranium-234.

Alpha pulse height analysis was examined as a possible alternate method of determining the isotopic ratios. Because of the low specific activity, ideally thin samples could not be prepared. Uranium-234 emits the most energetic alpha particles in the chain (72% at 4.768 Mev and 28% at 4.717 Mev). These peaks were studied to determine the effect of self-absorption on the shape of the spectrum. This information was used to correct the 4.370-Mev component of uranium-235 (25% of the uranium-235 alphas), subtracting the contribution of the higher- and lower-energy alphas from this peak.

The uranium-234 content of the sample as determined by alpha pulse height analysis was 0.99%.

NBS standard uranium (as U_3O_8) was analyzed in a similar manner, comparing the uranium-234 peaks to the 4.195-Mev peak from uranium-238. Results of this analysis gave 0.0053 wt % uranium-234, compared to the literature value of 0.0057%.

ANALYSIS OF STEARIC ACID IN SILVER POWDER

Previous efforts to determine stearic acid (inhibitor) concentration in the presence of silver powder (catalyst) failed because of the small percentage of stearic acid involved. Direct infrared analysis could not be used because of the strong absorptivity of the silver catalyst. The ATR (attenuated total reflectance)

[11] R. J. Jones (compiler), *Selected Measurement Methods for Plutonium and Uranium in Nuclear Fuel Cycle*, TID-7029.

technique was not applicable because the stearic acid concentration was below the limits of detection. Attempts at leaching stearic acid from the silver were not considered satisfactory.

Pyrolysis of the silver samples did provide useful information. Each organic material pyrolyzed produces different proportions of various lower-molecular-weight compounds. Without attempting to identify the materials that produce peaks on the chromatogram it is still possible to associate the overall pattern of peaks with a certain pyrolyzed compound. The pattern of peaks serves as a "fingerprint" in the same sense that an infrared spectrogram is a "fingerprint" identification of a material.

The pattern of peaks for stearic acid was obtained by passing pyrolyzed stearic acid products through a 1.5-meter silica gel column. When samples of the silver catalysts weighing from 0.13 to 0.17 gram were pyrolyzed the spectrum and the quantity of pyrolyzed products were found to be similar to that from 0.8 mg of stearic acid. The gas chromatographic method of evaluating the pyrolysis of silver powder thus served as a qualitative and rough quantitative analysis.

NUCLEAR MAGNETIC RESONANCE STUDIES

Tri-n-octylphosphine oxide (TOPO) has been found to be an excellent reagent for extracting uranium from waste solutions. The TOPO is dissolved in an organic solvent which forms a two-phase liquid system with the waste solution and carries the uranium over into the organic phase. Nuclear magnetic resonance (NMR) studies of uranium and other metals complexed with TOPO in carbon tetrachloride solution show that the change in chemical shift between the absorption peak of the methyl protons and terminal methylene protons of the TOPO molecule is directly proportional to the amount of metal complexed (see Table II).

Table II

CHEMICAL SHIFT BETWEEN METHYL AND TERMINAL METHYLENE PROTONS OF TOPO COMPLEXED WITH INCREASING QUANTITIES OF COBALT AS $CoCl_2 \cdot 6H_2O$

Chemical Shift (cps)	Concentration of $CoCl_2 \cdot 6H_2O$ Added to CCl_4-TOPO (0.10g/ml) Solution (mg/ml)
0	0.0
7	0.8
25	1.6
35	2.4
47	3.2
61	4.2
69	5.1
76	6.0
83	7.0
98	8.1
103	9.1
112	10.2
135	12.3
152	14.5
174	17.1
211	21.1
253	26.4
276	29.6

Table 11 indicates the change in chemical shift in cycles per second, between the methyl and terminal methylene group protons of TOPO complexed with increasing quantities of cobalt as $CoCl_2 \cdot 6H_2O$. Figure 15 is a plot of the data showing the chemical shift in arbitrary units.

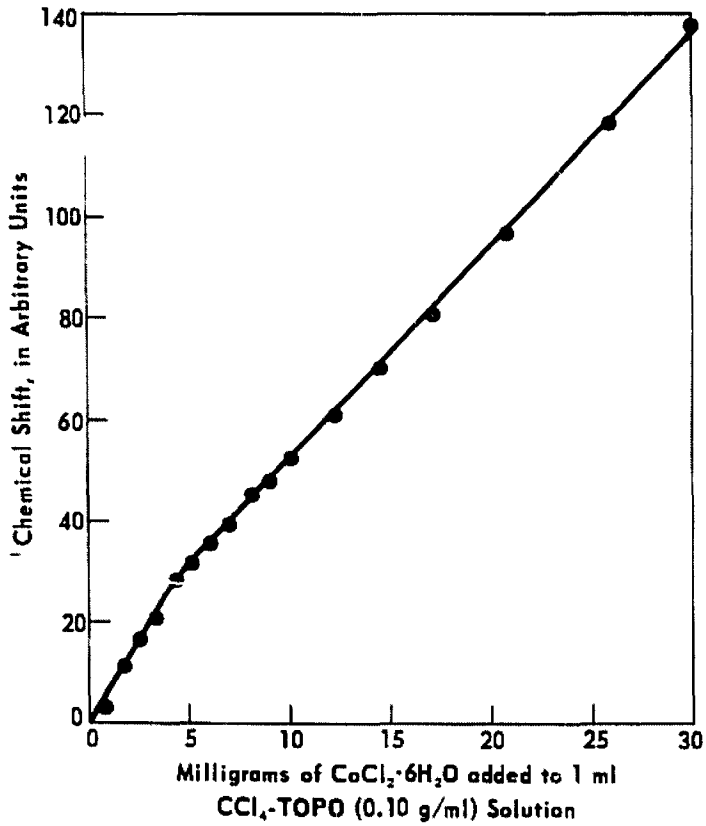

Figure 15. *Chemical Shift between Terminal Methyl Group Protons and Protons of the Methylene Group Adjacent to the Phosphorus Atom.*

SEMICONDUCTOR RADIATION DETECTORS

Recent advances in semiconductor detectors have shown that germanium surface barrier detectors may possess advantages over silicon detectors at cryogenic temperatures. Since germanium surface barriers are not commercially available, some detectors are being fabricated for use with low-temperature nuclear alignment experiments. Silicon surface barrier detectors are being prepared to gain experience in fabrication techniques.

Some surface barrier detectors were prepared by slicing a single crystal of N-type silicon parallel to the (111) plane to a thickness which is about 10 microns greater than the final desired thickness. The wafer was lapped and polished to the desired thickness, then etched to remove foreign particle inclusions. It was cleaned further in distilled water, then methyl alcohol, and finally distilled water. The wafer was then

put in br ng distilled water for 30 minutes; after removal it was blown dry with air and allowed to remain between . eets of filter paper overnight. An oxide (P-type) was thus formed on the surface to provide the barrier region.

The silicon wafers were mounted between Pyrex glass rings with epoxy and a 400A layer of gold was plated on both exposed surfaces, as shown in Figure 16. One surface was then chosen to be the face of the detector and an ohmic contact was made to the back with #22 tinned copper wire and silver conducting paint. This same paint was used t make the face contact to the container.

The performance of one of these detectors was acceptable, and a polonium-208-209-210 alpha spectrum was obtained to determine the characteristics of the detector. The resulting spectrum is shown in Figure 17.

A control circuit and drift oven, shown in Figures 18 and 19 respectively, were constructed. This system will be used for preparing lithium drift detector crystals.

CALORIMETRY

300-Watt Calorimeter A water bath calorimeter capable of assaying 450 watts of power has been constructed, calibrated, and used to assay 300-watt samples of polonium-210. The calorimeter is noteworthy primarily because of its simplicity. The precision probable error per observation is about 0.7 watt. The accuracy is not known, but from a consideration of the individual components, the error should be less than 0.5%. The basic method of operation was developed in February, 1956, to measure heat capacities. The resistance of the heater in the temperature controller is the only parameter of the calorimeter proper

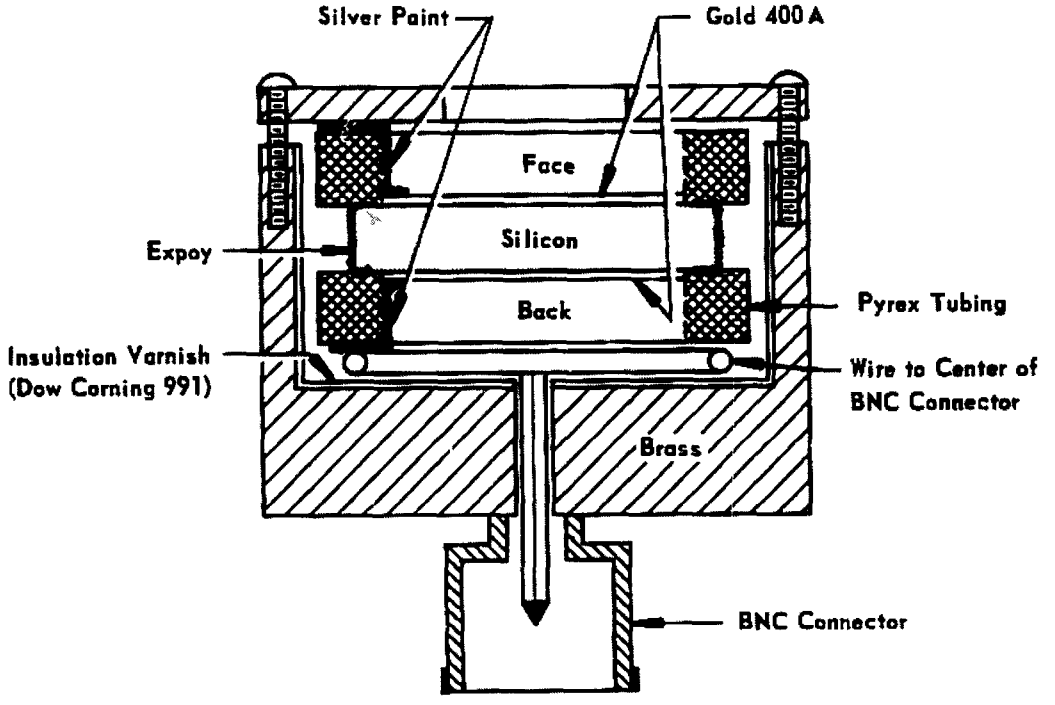

Figure 16. *Encapsulation of a Surface Barrier Detector*

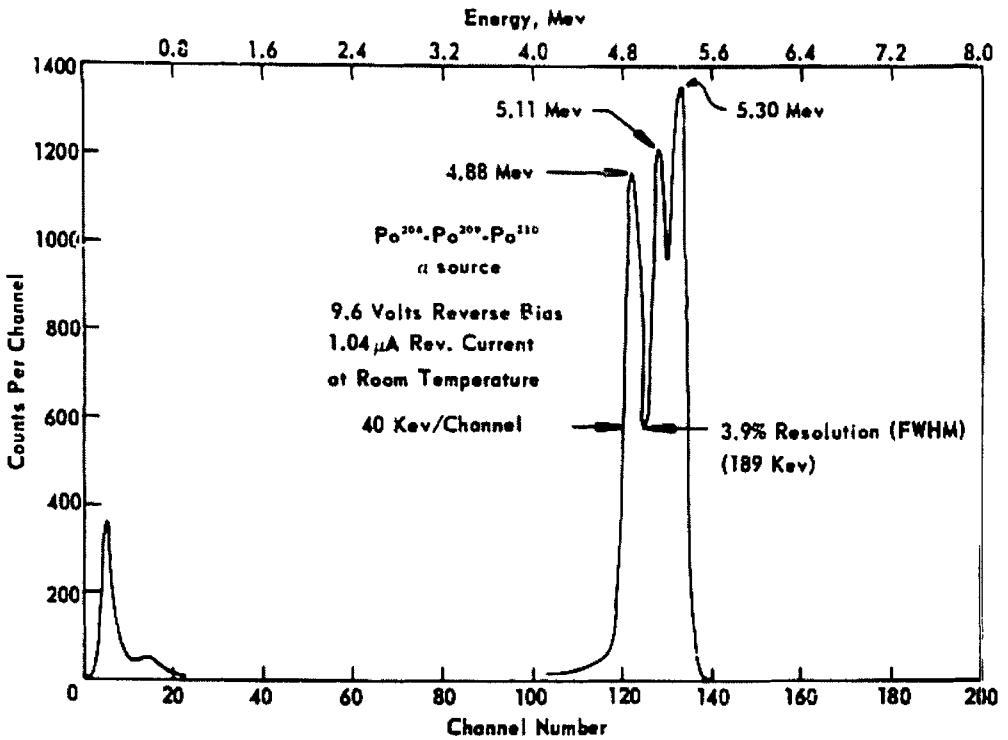

Figure 17. *Performance of a Surface Barrier Detector*

which enters the numerical calculations of sample power or energy. This simplification is achieved with temperature controllers and integrating calorimeters which are calibrated in a separate experiment. The temperature controllers can be used in three ways: (1) to maintain a null between sides of a differential calorimeter used to measure heat capacities; (2) to maintain a constant temperature difference between sides of a differential calorimeter used to measure power; and (3) to maintain an absolute temperature of a single-sided calorimeter, such as the one under discussion. In all three applications, the control heater is located in the sample side and is in series with the heater of the integrator. The output of the integrator can be greater or smaller than the calorimeter depending, among other things, on the relative heater resistances. A large power and temperature rise in the calorimeter proper can be reduced to a small temperature rise in the integrator, thus achieving a high degree of linearity with the possibility of safely making a large extrapolation beyond the highest calibration level. No d.c. equipment capable of calibrating a calorimeter at the 300-watt level was available at the time; therefore this technique was necessary to avoid using a.c. watt meters.

The physical arrangement of the 300-watt calorimeter is quite simple. The calorimeter proper consists of a conventional well-stirred bath maintained at a temperature of 80°C with a 300-watt mag-amp controller (described in the next section). About 315 watts are required to maintain this temperature. The 25-ohm control heater is in series with an 0.08-ohm heater in the integrator which is located in another temperature-controlled bath. The output of the integrator was measured with a potentiometer-galvanometer system.

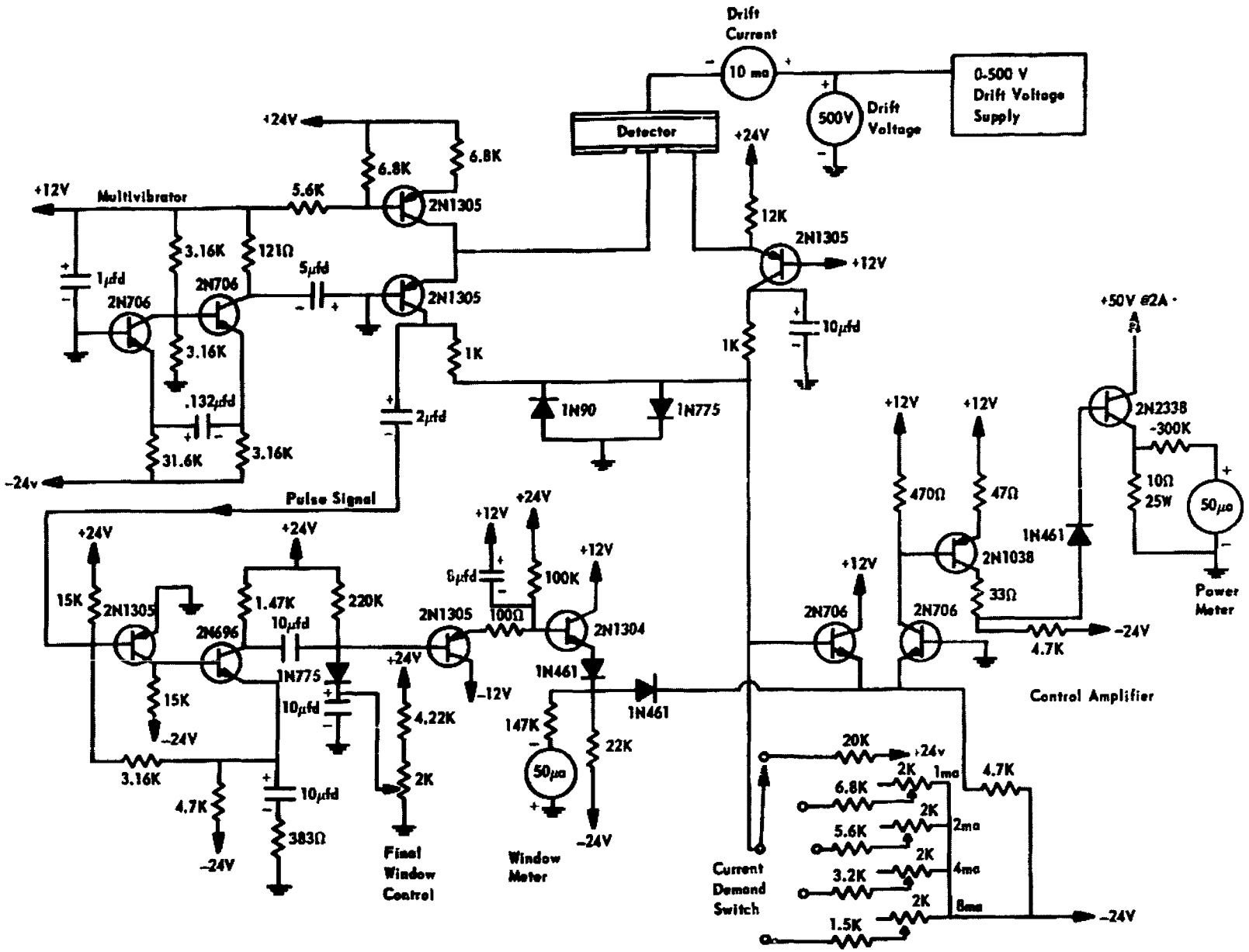

Figure 18. Control Circuit for Lithium Drifting Oven

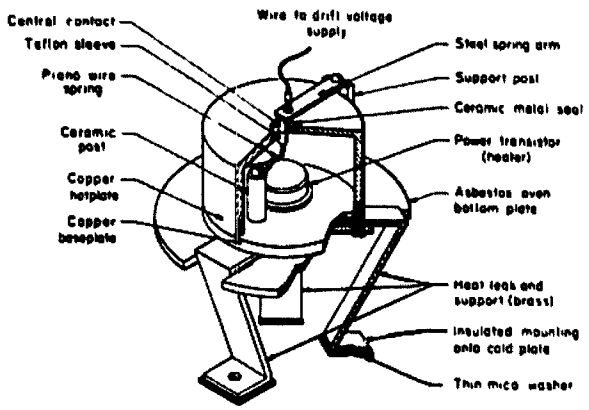

Figure 19. *Drifting Oven (Cutaway View)*

The resistance of the control heater (R_c) at 80°C was measured with 100ma d.c. with a conventional panel board. The sensitivity of the integrator(s) in microvolts/ampere was determined at 0.5 and 1.0 ampere, also with a conventional panel board.

The assay procedure is equally simple. The sample is suspended in the water by means of a hook attached to a 0.5-in. diameter lid in the cover of the bath. The bridge unbalance of the integrator is measured periodically for several hours and the equilibrium points are averaged to give E_s. The sample is replaced with a dummy sample. The integrator output is again measured for several hours and averaged to give E_o. The sample power is then calculated according to the following equation:

$$W_s = \frac{(E_o - E_s)R_c}{S} = I^2 R_c$$

The term $(E_o - E_s)/S$ is equivalent to I^2, where I is the average root-mean-square current flowing through the integrator and consequently through the control heater. $I^2 R_c$ is the real power in the heater if the heater impedance is purely resistive. Since the current in the heater is 60 cycles with few harmonics and the wire is bifilar-wound on non-magnetic materials, the reactive impedances are very low. The integrator design is a modification of previous integrators.[14] The heater is a 5-inch length of #16 manganin wire imbedded in the aluminum heater form and held in place by epoxy resin. The ends and central section of the thermel form were made of Kel-F. The 228-ohm bridge consists of a single layer of #37 enameled "99" alloy wound over the aluminum sections only. The time constants of the two components, thermel and heater, are the same as in previous integrators. The sensitivity of the integrator with 5 milliamperes bridge current and 0.5 and 1.0 ampere heater current was in each case equal to 1622.0 microvolts per ampere squared. This is equivalent to a temperature rise in the thermel of 0.53°C/ampere². At 300 watts the current through the 25.41-ohm calibrating heater and integrator is $(300/25.41)^{1/2}$ = 3.44 amperes, and the corresponding temperature rise in the integrator is 6.3°C. The sensitivity of a calorimeter, with the same bridge wire and air gap, decreases linearly by 0.45% from 0° to 6°C. The sensitivity of the integrator was assumed to fall off by the same amount and to result in a sensitivity of 1622/1.0045 = 1614.7 microvolts/ampere² at the 300-watt level. Equipment now on hand will permit calibration of the integrator to 3 amperes.

The control heater was constructed similarly to the tubular heater described previously. The heater wire is double-nylon covered #23 manganin. The heater resistance has been measured several times at different bath temperatures. All values fall within the first and last measurements: 25.513 ohms at 40°C on October 22, 1964 and 25.412 ohms at 80°C on December 9, 1964. The first two assays with this calorimeter were obtained with an 18-inch fan blowing air normal to the top of the water bath from a distance of 3.5 feet.

[14] MLM-CF-61-3-171.

It was thought that the fan would minimize the effect of people walking near the bath. However, the fan was discontinued and the stability of the calorimeter seemed unaffected. The only difference was a decrease of 77 watts in the control power. The heat transfer to the room from the bath is by conduction, radiation, convection, and evaporation. Evaporation can take place only around the stirrer shaft. Since about 8 quarts of water have evaporated from the bath in a month, the power loss from evaporation is about 6 watts. The variation in this wattage due to barometic pressure would be negligible in comparison to operation at 300 watts. Most of the heat transfer is by radiation and conduction to the room. Room temperature variations are therefore the chief cause of variations in the integrator output. Since the bath is elevated above room temperature by 55°C, a room temperature change of ± 0.25°C between sample and heater run can cause an error of 0.5%. The room in which the calorimeter is located is controlled to about this extent and thus accounts for the observed probable error of 0.7 watt, or 0.24%. It is important to note that any calorimeter at Mound Laboratory, including micro calorimeters and high-temperature calorimeters, can be operated by the same method which has been described here.

A thermoelectric integrator is being constructed, the thermopile being a single thermopile card as in the thermoelectric generator. It is hoped the reliability of these integrators will be commensurate with standard resistors, standard cells and potentiometers, thus obviating the need for calibration heaters in many applications.

Temperature Controllers The operation of calorimetric equipment at Mound Laboratory depends on the degree to which temperatures can be held constant with closed loop servo-control systems. Using a typical environmental water bath as an example, this servo-system (Figure 20) would consist of (1) a temperature sensor, a battery-driven Wheatstone bridge composed of two opposing arms of "99" alloy wire and two opposite arms of manganin wire, (2) an amplifying system capable of supplying full power with an input signal of approximately 15 microvolts, (3) the control heater which supplies heat to the water bath. The time constant of the system should be no greater than 20 seconds, and the system also has the property of amplifying only a negative signal, as this corresponds to a temperature lower than the control point.

The temperature-sensing element, a brass jacket with the sensing windings coiled on the inside surface, has the following construction. A water-tight brass jacket is made by machining a 1.500-in. ID by 1.750-in. OD piece of brass tubing to an outside diameter of 1.520 in.(0.010-in. wall thickness). A cap is soldered to the bottom end and a mounting flange to the top end, making an assembly approximately 15 in. long. The completed jacket is then nickel-plated on the outside to resist corrosion and galvanic action.

The sensing coils are first wound on a form, then inserted in the jacket, and the form is removed. The form, a 1/4-in. layer of Ceresin wax built up on an aluminum tube, is wound with double-nylon covered "99" alloy wire in a single layer containing two bifilar coils (each individual wire has a "lead" of four wire diameters). The outside diameter of the coils is selected to result in a tight slip fit to the jacket. The vertical length of the coil is not critical, but the greater the area of the winding the greater the averaging action of the bridge.

The top end of the winding is placed far enough below the top of the jacket so that room temperature effects do not enter into the operation of the sensing element.

To complete the construction, the empty brass jacket is heated to a temperature of approximately 50°C, which is the softening point of Ceresin wax. At that time the aluminum tube with Ceresin wax and wound wire is pushed slowly into the jacket until the end of the aluminum tube rests on the bottom of the jacket.

Heating is continued on the jacket until the wax is completely melted. Then the aluminum tube is withdrawn and the excess wax is poured off. This leaves the bridge wires lying against the inside of the jacket, relying for thermal contact on "hoop tension" and residual Ceresin wax. The "99" alloy arms, after balancing, form two opposite arms of a Wheatstone bridge, the other two arms being well-aged manganin resistors of the type found in commercially available decade resistance boxes. To isolate the windings from undesirable atmospheric effects the unit is hermetically sealed by means of a deeply recessed jacket lid. A multi-pin glass-to-metal seal is soldered in a hole in the bottom of the recessed jacket lid, and the manganin resistors and "99" alloy wire ends are soldered directly to the pins. When the lid is assembled to the jacket (with a rubber gasket) the temperature-sensitive connections are 3 to 4 in. down from the flange and well isolated from room temperature variations. The set or balance point of this bridge can be changed by externally shunting one of the arms with a precision decade resistance box.

The amplification system currently used (Figure 20) consists of a Leeds and Northrup electronic null detector, an intermediate Airpax magnetic amplifier, and a Minneapolis-Honeywell 150-watt magnetic amplifier. An attenuating network is provided by which one can select the percentage of the power amplifier output reaching the servo heaters.

Adjustment of the mag-amp servo-control system is accomplished by the following procedure. To prevent damage to the units the load must be connected across the output terminals of amplifier 3 before the amplifier is turned on.

Procedure:

1. With amplifiers 1 and 3 off, adjust mechanical "zero" of all meters.
2. All amplifiers are turned ON.
3. With input connected to amplifier 1 but with battery disconnected from bridge, adjust electrical "zero" of amplifier 1. Then adjust potentiometer inside amplifier 3 so that meter M4 reads 5-10 volts.
4. Using a large signal so that amplifier 1 is off scale to the left, adjust R-24 so that meter M4 reads 70 volts.
5. Using a signal that will cause amplifier 1 to offset 2-1/2 large divisions to the left, adjust R-22 so that meter M4 reads 50 volts.

Control heaters contain large-diameter copper wire connected to the end of the manganin wire coil and placed in close thermal contact with the inside of the jacket. This arrangement allows all the heat generated in the manganin windings to flow into the water, minimizing heat loss to the room, and also permits the construction of a four-terminal calibration resistor whose resistance can be measured under load.

More recently the control heaters were positioned concentrically with the bath stirrer and shaft. Manganin wire is bifilar-wound on the smaller of the inner cylindrical surfaces of a double-walled jacket having wall thicknesses of approximately 0.010 in. The water-tight jacket whose innermost diameter is slightly larger than the propeller diameter has a length approximately the same as its outermost diameter, and is located concentrically around the stirrer shaft so that the lower end of the jacket is just above the propeller. The heat flowing into the high-velocity water is mixed and distributed evenly to the bath at a faster rate than

can be accomplished with the original tubular heaters. Although the combination of low-mass coils in good thermal contact with the thin-walled jacket produces sensing elements and heaters of fast response time, the real virtue of this type of construction is the stress-free positioning of the wire, resulting (especially in the case of sensing elements) in very stable units. Two water baths using this type of unit have not drifted in temperature more than 0.002°C in two years.

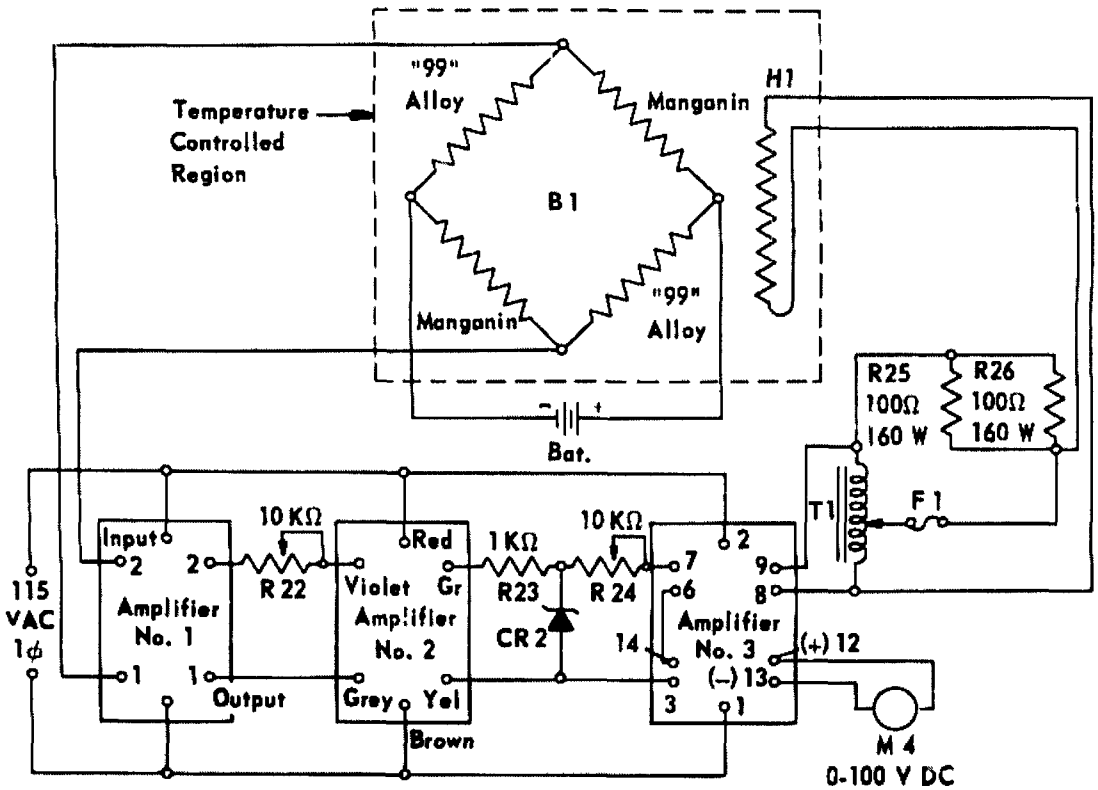

Figure 20. *Amplification System*

Components of the Amplification System:

Amplifier	**#1:**	**Electronic D.C. Null Detector, L&N Model 9834-2**
	#2:	**Amplifier, Magnetic, Airpax Model M-5267-R**
	#3:	**Amplifier, Magnetic, Minneapolis-Honeywell #365235-3**
B1		**Sensing Element-Calorimeter Bath**
BAT		**Battery, Low-Discharge, Willard #DD-5-3**
CR2		**Diode, Zener, 5v, 20 ma, 1N751-A**
F1		**Fuse, 3a, 125v**
H1		**Heater, Immersion, 230v a.c., 200W**
M4		**Meter, 0-100v d.c., Triplett Model 320-M**
R23		**Resistor, Carbon, 1000Ω, 1/2W**
R22 &R24		**Resistor, Molded Composition, Variable, 10,000Ω, 2W**
R25		**Resistor, Wire-Wound, 100Ω, 160W**
R26		**Resistor, Wire-Wound, 100Ω, 160W**